Nano Research
2021, 14(6): 1609–1624

ISSN 1998-0124 CN 11-5974/O4
https://doi.org/10.1007/s12274-020-3050-z

Review Article

# Space-confined growth of metal halide perovskite crystal films

Linyi Li, Jinxin Liu, Mengqi Zeng, and Lei Fu (✉)

*Country College of Chemistry and Molecular Sciences, Wuhan University, Wuhan 430072, China*


**Received:** 20 June 2020 / **Revised:** 9 August 2020 / **Accepted:** 10 August 2020

## ABSTRACT

Metal halide perovskites, as a new generation of optoelectronic materials, have attracted a great deal of interest due to their remarkable intrinsic properties. Due to the excellent optoelectronic properties, the perovskite crystals are widely used in lasers, photodetectors, X-ray detectors and solar cells. Considering the device performance and fabrication requirements, proper thickness of the crystal is required to avoid carrier loss and simultaneously ensure sufficient light absorption, which can realize the full potential of its excellent carrier transport property. Thus, the fabrication of perovskite crystal in a thin film with an adjustable thickness is highly desirable. The space-confined method has been demonstrated to be an effective way of preparing perovskite with controlled thickness. In this method, the thickness of perovskite can be regulated flexibly in a geometric confined space. Moreover, the size, quality and architecture of perovskite crystal films are also major concerns for practical photoelectric devices, which can also be optimized by the space-confined method owing to its good adaptability towards various modified strategies. In a word, the space-confined method is not only a simple and conventional way to adjust the thickness of perovskite crystal films, but also provides a platform to optimize their size, quality and architecture through applying appropriate strategies to the confined space. Herein, we review the space-confined growth of perovskite crystal films. Particularly, various modified strategies based on the space-confined method applied to the optimization of thickness, size, quality and architecture are highlighted. Then the stability investigating and component regulating of perovskite crystal films would be also mentioned. Furthermore, the correlation between the perovskite thickness and the device performance is discussed. Finally, several key challenges and proposed solutions of perovskite thin films based on the space-confined method are discussed.

## KEYWORDS

space confinement, metal halide perovskite, thickness adjustment, controllable preparation

## 1 Introduction

Metal halide perovskites have received intensive research interest due to their outstanding optoelectronic properties, including wide absorption range [1], high extinction coefficient [2], long electron-hole diffusion length [3], high carrier mobility [4, 5] and so on. Benefitting from these excellent properties, perovskites are promising candidates for constructing high-performance solar cells [6, 7] and photodetectors [8]. Thereinto, the photoelectric conversion efficiency of the device is mainly determined by two steps: light absorption and charge transfer, both of which are highly correlated with the crystal thickness. Specifically, the excessive thickness of bulk perovskite crystals would prolong the transit time of photon-excited carriers and increase the recombination probability, thus causing unnecessary carrier loss. On the contrary, the reduction in thickness would result in poor light absorption and thus the device performance will be greatly degraded [9–11]. In this regard, an ideal perovskite film for the construction of high-performance devices means that the thickness needs to be controlled at an appropriate level. Thus, a method to prepare perovskite crystal films possessing suitable thickness is highly desirable and intriguing to boost device performance.

So far, various methods have been developed to prepare perovskite crystal films, such as cavitation triggered asymmetrical crystallization [12], vapor phase epitaxial growth [13, 14] and top-down method [15]. Among them, due to the large difference between the solubilities of precursors, cavitation triggered asymmetrical crystallization method, is not compatible with the growth of iodide-based perovskite films, such as $CH_3NH_3PbI_3$ ($MAPbI_3$). The vapor-phase epitaxial growth is a powerful technique to grow high-quality perovskite crystal thin films [13]. However, to achieve high quality, both high temperature and suitable lattice-matched epitaxial substrates are extremely required, which may be detrimental to extensive applications in terms of convenience and simplicity. Besides, the top-down method has been demonstrated as a reliable and controllable approach to slicing large crystals into thin wafers [15, 16]. Certainly, it will inevitably induce surface defects, and further reducing thickness may lead to the fragmentation of crystals [9].

The space-confined method, as a promising way, possesses relatively moderate conditions and without strict limitations, which can potentially be applied to the growth of various halide perovskite crystal thin films. It is the most commonly adopted strategy to obtain perovskite crystal film with a controllable thickness. In this way, the perovskite precursor solution is constrained into a thin film format by equipping geometric space confinement. And the thickness could be adjusted flexibly by altering the geometric space. The feature of thickness-control endows a unique advantage to tailor the perovskite crystal films for distinctive optoelectronic applications. Additionally, based on the space-confined method, the size,

Address correspondence to leifu@whu.edu.cn

quality and architecture of the film could be further improved by applying additional optimizing strategies in such a confined space, which can also significantly affect the performance of the fabricated photoelectric devices. Using the space-confined method with various modified strategies, desirable perovskite films with controlled thickness, enlarged size, improved quality and tailored architecture have been fabricated. Besides, the space-confined method has the advantage of substrate-independent growth, which indicates little restrictions on the choice of substrates. It facilitates direct integration of perovskite films with desired substrates, resulting in easier fabrication and optimization of the device [17, 18].

In this review, we will introduce the compatibility between the space-confined method and conventional perovskite crystal growth methods, which successfully changed the form of perovskite from bulk to film. Then, according to different expectations, various modified strategies based on the space-confined method are highlighted, such as thickness adjustment, size enlargement, quality improvement and architecture tailoring. Subsequently, more possibilities for improvement of perovskite crystal films based on the space-confined method would be also mentioned, including stability investigating and component regulating. Furthermore, the correlation between the perovskite thickness and the device performance is discussed. Finally, several key challenges and proposed solutions of perovskite thin films based on the space-confined method are discussed.

## 2 Compatibility of space-confined method

The space-confined method has good compatibility with other conventional perovskite crystal growth methods, which can meet the needs of perovskite thin film growth [19]. In the space-confined method, the introduction of geometric confined space is the core of the whole method. The geometric confined space can be easily applied in the process of crystal growth and restrict the growth direction of crystal directly, which ensures the lateral growth of the crystal. The unique feature of the space-confined method is its compatibility with the traditional perovskite crystal growth methods.

Up to now, various fabrication methods have been extensively studied for preparing perovskite crystal, including inverse temperature crystallization [20, 21], cooling-induced crystallization method [22], antisolvent vapor-assisted crystallization [23] and top-seeded solution-growth method [3]. Considering the virtue of these mature preparation technology based on the solution process of perovskite crystal, the concept of confined space is introduced into the process of perovskite crystal growth to obtain a thin film format. By combining various traditional methods of perovskite crystal growth with the space-confined method, the perovskite crystal could be successfully transformed from bulk perovskite crystal to a thin film format. It can be found that the space-confined method can be compatible with a variety of conventional methods. Specifically, as shown in Fig. 1, the precursor solution is restricted between two substrates, and then the perovskite crystal film is grown according to the conventional growth method of perovskite crystal. In this way, the expected perovskite crystal with a thin film format was prepared.

The corresponding growth results are exhibited as follows: When the space-confined method was combined with the top-seeded solution growth method, the thickness of the resulting $CH_3NH_3PbBr_3$ ($MAPbBr_3$) crystal film could be adjusted from 13 nm to 4.5 μm [24]; when incorporating the confined space into antisolvent vapor-assisted crystallization, the single-crystal $(C_6H_5C_2H_4NH_3)_2PbI_4$ thin films with the lowest thickness of 1 μm was achieved; the combination of the space-confined method with cooling-induced crystallization method can prepare quasi-two-dimensional (2D) $BA_2MA_2Pb_3I_{10}$ single crystals with a thickness of 20 μm [25]; for inverse temperature crystallization based on space-confined method, the thickness of resultant single-crystal wafer of $MAPbI_3$ could be controlled to as thin as 35 μm [26]. As illustrated in Fig. 1, the space-confined strategy can act in synergy with most of the conventional perovskite crystal growth methods, such as the top-seeded solution growth method, antisolvent vapor-assisted crystallization method, cooling-induced crystallization method and inverse temperature

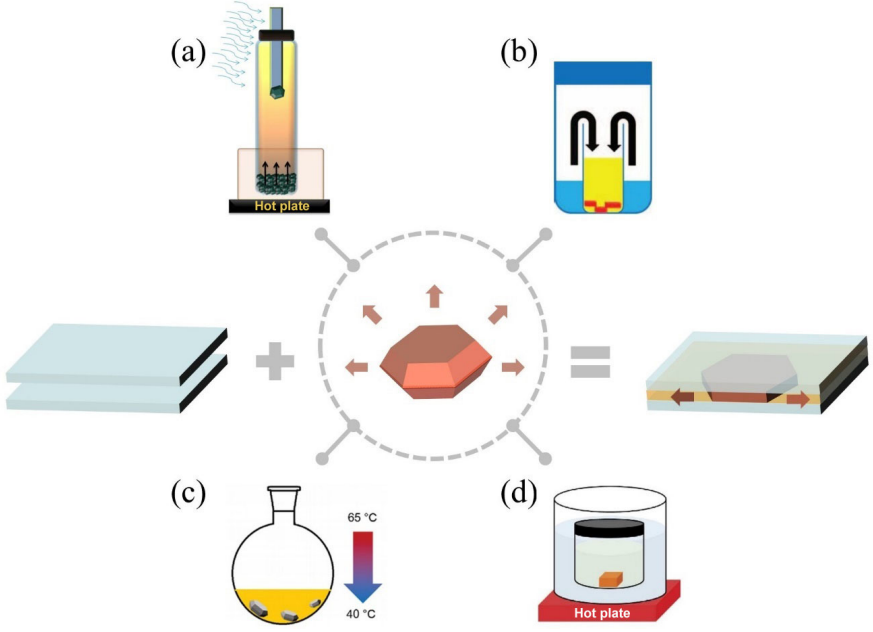


**Figure 1** The compatibility of space-confined method with various conventional perovskite crystal growth methods. (a) Top-seeded solution growth method. Reproduced with permission from Ref. [3], © American Association for the Advancement of Science 2015. (b) Antisolvent vapor-assisted crystallization method. Reproduced with permission from Ref. [23], © American Association for the Advancement of Science 2015. (c) Cooling-induced crystallization method. Reproduced with permission from Ref. [22], © The Royal Society of Chemistry 2015. (d) Inverse temperature crystalization method. Reproduced with permission from Ref. [20], © Macmillan Publishers Limited 2015.

crystallization method, to prepare specific perovskite films with suitable thickness. The combination between the space-confined method and conventional growth methods of perovskite crystals can afford successful transformation from bulk perovskite crystals to thin films of various perovskites.

In addition, the results of perovskite crystal growth with/without space limitation were compared [27]. The crystal wafer based on the space-confined method shows a hexagonal shape, which is consistent with the top view of the large size perovskite crystal prepared without space limitation. This indicates that the space-confined method only confines the direction of crystal growth, while the crystal-growth habit is not altered. Clearly, without confinement using in the method, crystals with normal geometries are harvested.

## 3 Adaptability of space-confined method

The space-confined method exhibits decent adaptability with various modified strategies to alter the growth process of perovskite crystal films, in which numerous growth conditions can be altered in a confined space, including the wettability, structure and spacing of two substrates, the diffuse rate of the precursor, the solubility and evaporation rate of the solvent, and so on. Taking advantage of these facile modifiable features in the space-confined method, the optimization of thickness, size, quality and architecture of perovskite crystal films could be realized. Here, various strategies would be discussed for modifying the space-confined growth method, to fabricate perovskite crystal films with controlled thickness, enlarged size, improved quality and tailored architecture.

### 3.1 Thickness adjustment of perovskite crystal films

The thickness of perovskite crystal film is particularly critical to the constructed photoelectric applications. Since the thickness significantly affects light absorption and carrier recombination of the crystals, perovskite films with favorable thickness would dramatically enhance the device performance. However, owing to the intrinsic isotropic growth behavior, the resulting product is often a bulk instead of a film, which would increase the difficulty in fabricating high-performance devices.

To prepare perovskite thin films, an anisotropic growth environment is required to break the isotropic growth condition. Thus, the space-confined method with the ability to reduce and adjust the crystal thickness has attracted enormous attention. In this method, a confined space restricted the vertical growth of crystals is employed, which enables the synthesis of perovskite film with a controllable thickness. In this part, we focus on strategies for adjusting the thickness of perovskite crystal films based on the space-confined method.

The thickness of perovskite crystal film can be controlled directly by altering the distance between the two substrates. Usually, two substrates aligned in parallel are separated by spacers to form a gap. By controlling the size of the spacer which could adjust the distance between two substrates, Rao et al. obtained perovskite crystal films with a thickness range of 100–800 μm [28]. As shown in Fig. 2(a), in a customized mechanical device, the U-style polytetrafluoroethylene (PTFE) thin membrane acts as a spacer, and its thicknesses are defined to 100, 200, 400 and 800 μm, which accurately determine the thickness of resulting perovskite crystal films.

Although thickness can be regulated by the spacer directly, the thickness of the prepared film is still at the millimeter level. In this regard, the pressure is applied to the confined space to further reduce the thickness. By adjusting the pressure, the film thickness can be tuned to the micron level or even to the nanoscale. Chen et al. and Yang et al. applied pressure on the confined space respectively [11, 24]. The device that supplies and measures the pressure is shown in Fig. 2(d). Atomic force

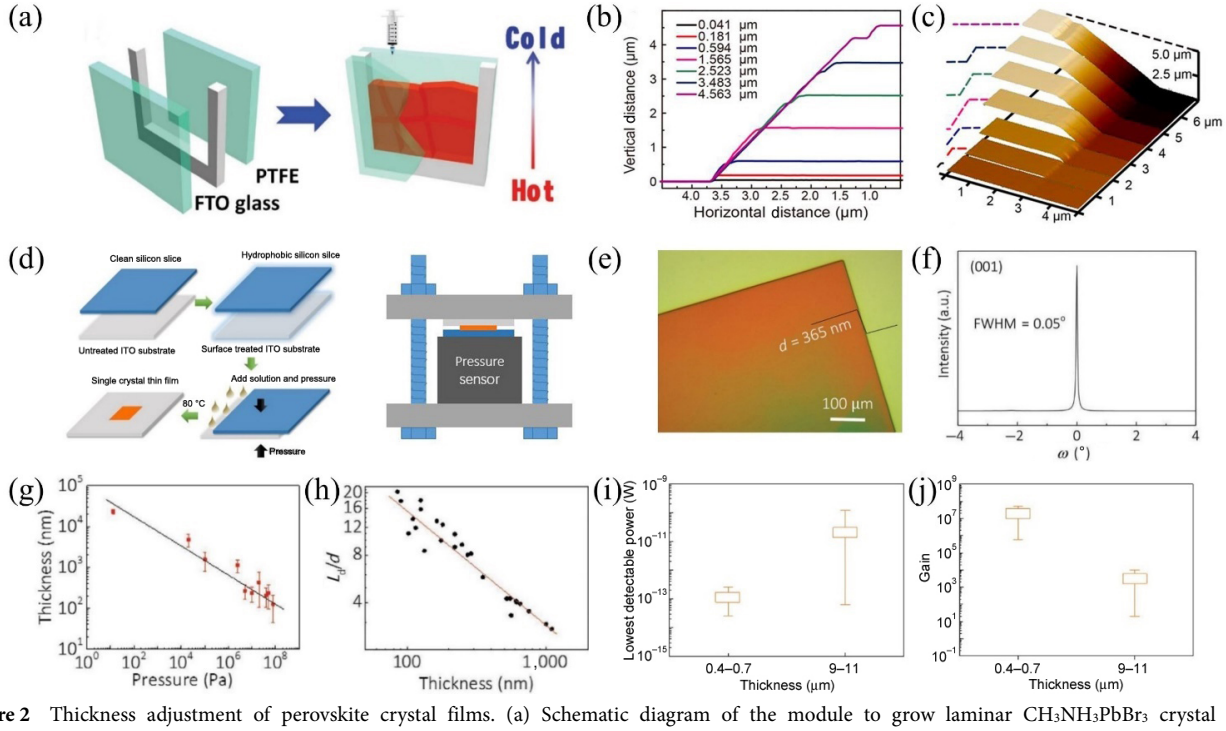


**Figure 2** Thickness adjustment of perovskite crystal films. (a) Schematic diagram of the module to grow laminar $CH_3NH_3PbBr_3$ crystal films. Reproduced with permission from Ref. [28], ©WILEY-VCH Verlag GmbH & Co. KGaA, Weinheim 2017. (b) and (c) AFM profiles and 3D images of $MAPbBr_3$ single-crystal thin films in various thicknesses. Reproduced with permission from Ref. [24], ©American Chemical Society 2016. (d) The schematic diagram of the growth process and pressure measurement device. (e) The optical image of a single-crystalline perovskite thin film with a thickness of 365 nm. (f) The full width at half-maximum of the (001) peak. (g) The thickness of the film varies with different pressure. (h) The ratio of diffusion length over film thickness versus film thickness. (i) and (j) Perovskite thickness-dependent performance: averaged minimum detectable power and maximum gain. Reproduced with permission from Ref. [11], © WILEY-VCH Verlag GmbH & Co. KGaA, Weinheim 2018.

microscopy (AFM) profiles (Fig. 2(b)) and three-dimensional (3D) images (Fig. 2(c)) reveal the successful fabrication of $MAPbBr_3$ single-crystal thin films with thickness ranging from a few nanometers to micrometers. A perovskite crystal film with 365 nm thick is shown in Fig. 2(e). And the high crystallinity can be observed according to the strong and sharp diffraction pattern in Fig. 2(f). As shown in Fig. 2(g), the thickness of the film is negatively correlated with the pressure applied to substrates, which demonstrates the decisive role of pressure in thickness control. And the thickness can be reduced to 100 nm under 108 Pa. Figure 2(h) shows the trend of the ratio of carrier diffusion length to film thickness with the thickness. The carrier diffusion length is much longer than the thickness, and the ratio decreases with the increase of the thickness, indicating that the thinner film is more conducive to carrier collection.

Furthermore, the thickness-dependent performance of the as-fabricated photodetectors was also systematically studied. Specifically, devices with thickness ranges of 400–700 nm and 9–11 μm were measured for comparison. The statistical results of the averaged minimum detectable power and the maximum gain in the two thickness ranges are shown in Figs. 2(i) and 2(j). It can be concluded that the device with a thinner film has much better performance than the thicker one. As the thickness decreased from about 10 μm to hundreds of nanometers, the lowest detectable power and internal gain were improved by two and four orders of magnitude respectively. For the weak signal detection, the thinner thickness is beneficial to reduce the recombination probability and enhance the collection efficiency of carriers. And for the gain, the thinner thickness would shorten the transit time of carriers and consequently achieve a higher gain. Moreover, the thickness of the active layer could be further optimized to the best state to compromise the tradeoff between light absorption and carrier collection.

As mentioned above, the device performance has a close correlation with the crystal thickness. Through the methods mentioned above, including adjusting spacer size and applying pressure to the substrate, the thickness can be controlled to achieve an optimal device performance.

For the thickness control of perovskite crystal films based on the space-confined method, adjusting the distance between substrates by spacer is a simple and direct way to control the thickness. However, due to the limitation of the spacer size, the thickness is still at the millimeter level, and further thickness reduction is hindered. To obtain thinner perovskite crystal films, the pressure is introduced into the confined space, and the thickness can be altered from millimeters to micrometers or even nanometers. However, the introduced pressure does increase the preparation cost and equipment complexity. Thus, a facile and effective strategy based on the space-confined method needs further development.

### 3.2 Size enlargement of perovskite crystal films

Generally, a typical crystallization process contains two steps: nucleation and subsequent crystal growth, both of which play a decisive role in size control of perovskite crystals. For instance, the presence of excessive crystal nucleus would reduce the size of crystals, and the insufficient supply of precursors is hard to extend the subsequent crystal growth period to increase the size of crystals. In this section, various strategies based on the space-confined method would be discussed in controlling both nucleation and subsequent crystal growth to enlarge the size of perovskite crystal films.

#### *3.2.1 Controllable nucleation*

Random nucleation is a common issue in the process of crystal growth, and high nucleation density would hinder the enlargement of crystal size. For perovskite, due to the large difference between solubilities of precursors in the solvent, the one with lower solubility precipitates quickly during the solvent evaporation and behaves as growth seeds, leading to the random nucleation [29, 30]. This would induce the emergence of grain boundaries, which contribute to low carrier mobility and high recombination possibility and then degrade the device performances [31]. To suppress the random nucleation in the confined space, specific perovskite seeds need to be introduced into the liquid film system. In this part, much attention would be paid to the nucleation process control for large size film formation.

Yue et al. reported the seeded space-confined method for the first time [32]. They incorporated a seed $CH_3NH_3PbI_3$ crystal within a confined space, and the presence of this introduced seed inhibited random nucleation and facilitated the crystallization process. The obtained crystal plate has a thickness of 50 μm and a lateral dimension of up to 2 mm. In 2019, Gao et al. combined the space-confined growth and seed-induced crystallization method (Fig. 3(a)), and perovskite wafers as large as 10 mm have been successfully grown (Fig. 3(c)) [33]. In contrast, the crystal size is less than 3 mm without nucleation control in the space-confined growth method (Fig. 3(d)).

Furthermore, the space-confined growth method and the top-seeded solution-growth method were incorporated for growing large single-crystal $MAPbI_3$ perovskite wafers, as shown in Fig. 3(e) [24]. And hybrid perovskite single-crystal thin films with a size of submillimeter were fabricated (Fig. 3(f)). In the growth process, the introduction of the temperature gradient is a key factor for this space-confined method. The bottom solution stays saturated, while the top solution is supersaturated and crystallized due to the relatively low temperature, which provides the crystal nuclei for perovskite growth. Simultaneously, the temperature gradient would drive the solution convection, providing a continuous supply of precursors to ensure the continuous growth of perovskite crystal film.

Considering the scale and convenience of actual production, Gu et al. reported the selective growth of an $MAPbBr_3$ single-crystal thin film array with millimeter size via a seed printing strategy based on the space-confined method (Fig. 3(g)) [34]. The patterned perovskite seeds used in this method are shown in Fig. 3(h). Figures 3(i) and 3(j) show the crystallization results of the random and controllable nucleation in the system without and with introduced seed crystals respectively. The comparison between them shows that random nucleation is effectively inhibited by the introduced seeds, resulting in the controllable growth of perovskite single-crystal films in batches. In this method, the key is the introduction of printed seed array. The arranged seeds have a decisive effect on the array formation, since they can effectively inhibit the random nucleation and trigger the subsequent growth of perovskite crystal films. And the suppression ability of random nucleation could be controlled by the distance of seeds. As shown in Fig. 3(k), there is a significant correlation between seed distance and the ability to inhibit random nucleation. By the way, the obtained perovskite single-crystal films could be transferred perfectly to arbitrary substrates through the seed printing process, which is conducive to fabricate practical photoelectric devices.

The surface treatment of substrates is also a facile and effective way to control the nucleation density. Through selective surface treatment, the nucleation barrier of substrates can be altered flexibly, so as to achieve *in situ* controllable growth on the target substrate. For instance, in the work of Yang et al., they used

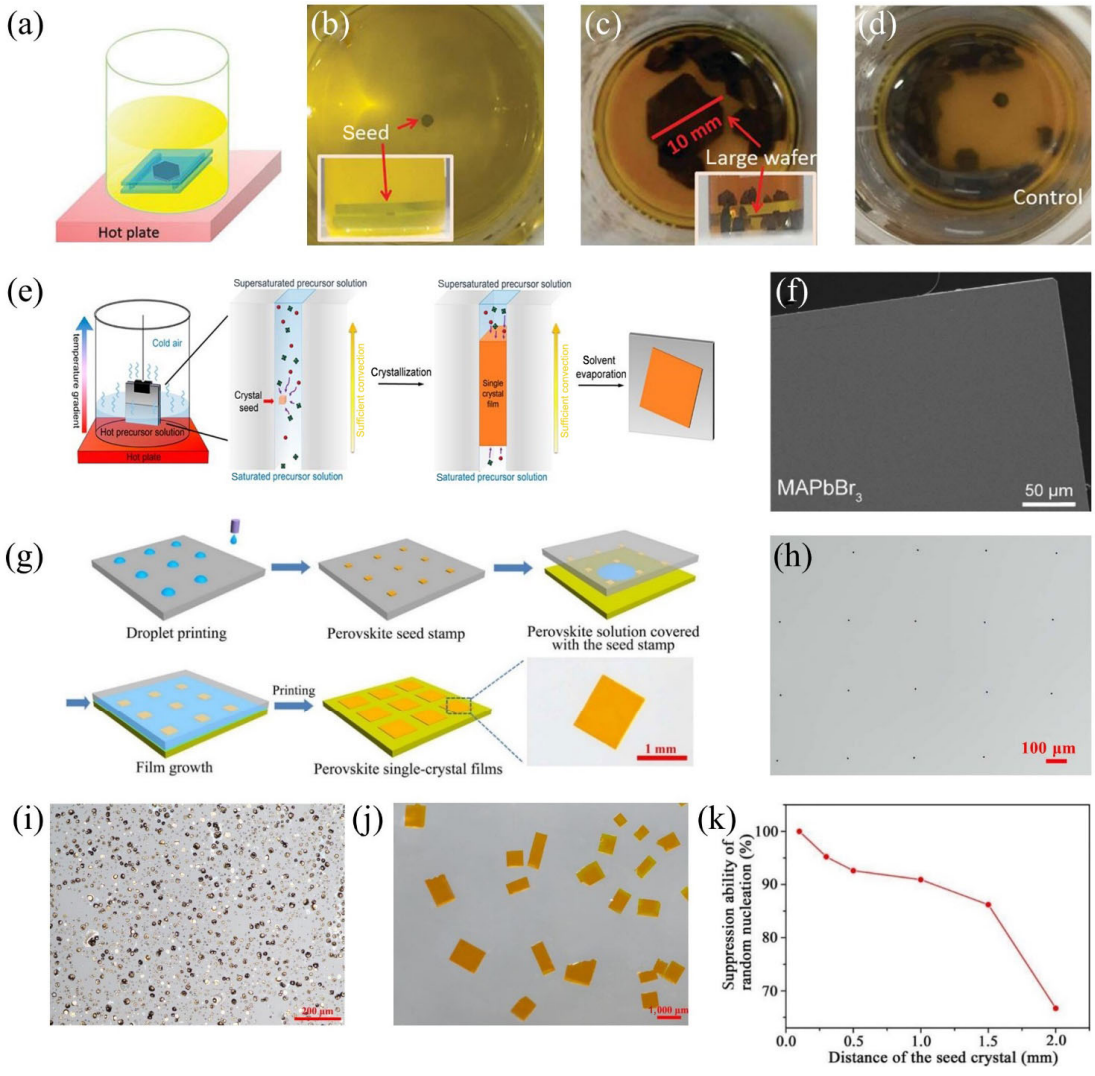


**Figure 3** The space-confined method incorporated with crystal seeds. (a) Scheme for seeded space-limited method. (b) and (c) The seed/product in the growth process using a combination of the space-confined method and seed-induced method and their cross-section views (inset). (d) The product of the growth using the space-confined method alone. Reproduced with permission from Ref. [33], © The Royal Society of Chemistry 2019. (e) Scheme for perovskite crystal film growth by top-seeded solution-growth based on the space-confined method. (f) SEM image of $MAPbBr_3$ single-crystal thin film. Reproduced with permission from Ref. [24], © American Chemical Society 2016. (g) The scalable growth of perovskite single-crystal film array by seed printing. (h) Optical image of the patterned perovskite seeds for the growth of perovskite single-crystal films. Optical microscopy images of the crystallization result of the random (i) and controllable (j) nucleation in the system without/with introduced seed crystals. (k) Suppression ability of random nucleation as a function of the distance of seeds. Reproduced with permission from Ref. [34], © American Association for the Advancement of Science 2018.

silicon wafer and indium tin oxide (ITO) as substrates to form a confined space and expected to grow perovskite crystal films on ITO via a space-confined method [11]. Hydrophobic treatment can increase the nucleation energy barrier, while hydrophilic treatment reduces the nucleation energy barrier. Therefore, to control the nucleation density, the two substrates were treated differently according to the expectation. Specifically, hydrophobic treatment was carried out on the silicon surface to increase the nucleation energy barrier, while oxygen plasma was used to treat ITO, which reduced the nucleation barrier on the ITO surface and activated the dangling bond on its surface. After that, the perovskite crystal film was more inclined to nucleate and grow on the surface of ITO. Moreover, the stronger interaction between the prepared perovskite and ITO makes the easier removal of the silicon chip for the subsequent construction of devices.

To conclude, the ability to manipulate the nucleation process, including the addition of crystal seeds, the introduction of a temperature gradient and the treatment of the substrate surface, is crucial to achieve perovskite crystal film with a large area controllably and repetitively.

### 3.2.2 *Continuous growth*

Typically, the growth of crystals would deplete the precursor, which hinders the subsequent crystal growth. In a confined space, the long-range transport efficiency of precursor ions is limited, which makes it hard to maintain further lateral growth of the crystal [18]. Therefore, to increase crystal size, it is necessary to accelerate the diffusion rate of precursor ions in such a confined space. In this part, from the perspective of the precursor solution dynamic flow and substrate wettability, some strategies are introduced to enlarge the crystal size by increasing the diffusion rate of precursor ions.

In 2016, Liu et al. designed an ultrathin geometry-defined dynamic-flow reaction system to grow single-crystal films of $MAPbI_3$ [27]. As schematically shown in Fig. 4(a), the ultrathin confined space is provided by a gap between two substrates, and the dynamic flow is achieved using a peristaltic pump.

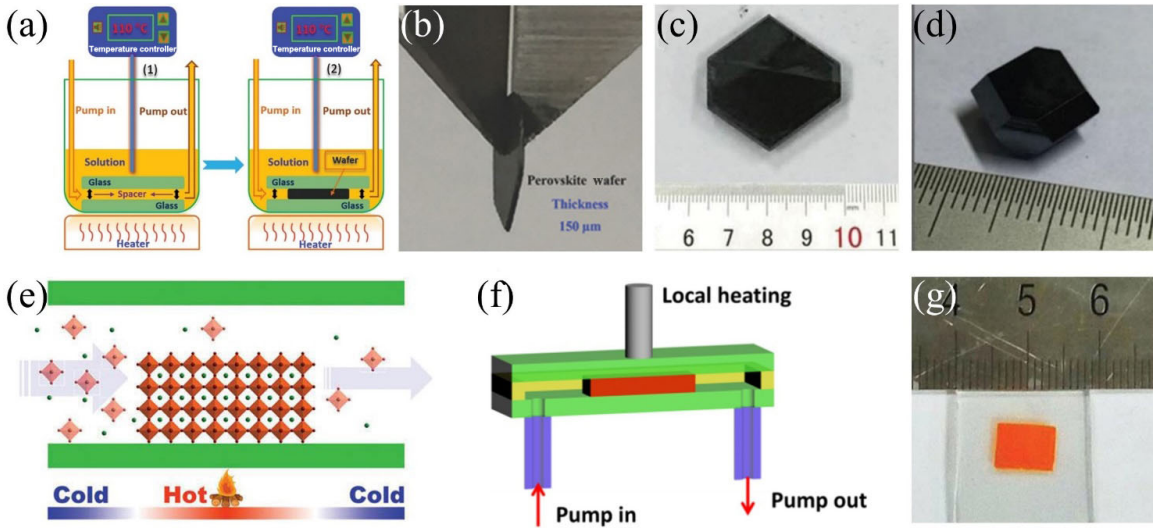


**Figure 4** The space-confined method incorporated with dynamic flow. (a) Schematic illustration for the ultrathin single crystal wafer preparation. Photos of perovskite wafers (b) with 150 μm thick and (c) and (d) with/without space limitation. Reproduced with permission from Ref. [27], © WILEY-VCH Verlag GmbH & Co. KGaA, Weinheim 2016. (e) and (f) Schematic diagram of the growth module with local heating. (g) The photo of the laminar $MAPbBr_3$ single crystal with a size of 6 mm × 8 mm. Reproduced with permission from Ref. [35], © The Royal Society of Chemistry 2017.

The resultant single crystal wafer of $MAPbI_3$ possesses a relatively large lateral size of up to centimeter (Fig. 4(c)), and the thickness could be adjusted with the assistance of sandwich spacers from 150 to 1,440 μm. In the process of crystal growth, on the one hand, the limited space confines the crystal growth within the slit channel, which ensures the lateral growth of crystals. On the other hand, the dynamic flow not only efficiently improves mass transport but also enables a constant fresh solution for continuous crystal growth. Besides, the thickness of the single crystal is determined by the distance between two glass slides. It is particularly noteworthy that in this system, the dynamic flow could continuously bring a fresh solution to replenish the precursor depleted by crystal growth, effectively avoiding the issue of insufficient precursor ions supply resulting in small crystal size.

Based on a similar approach, an optimized 16 μm thick laminar $MAPbBr_3$ was achieved after employing an ultrathin PTFE spacer [35], which is much thinner than the film mentioned above. The substrate is supplied with local heating as shown in Fig. 4(f). The local heating is employed to confine the nucleation position and thus the crystals primarily grows in the hot region (Fig. 4(e)). The continuous dynamic flow is the key to maintain the growth of single-crystal films. By the way, the leakproof nature of the module is extremely necessary to keep the precursor solution flowing and thus maintain the lateral growth of perovskite crystal films. In short, based on the space-confined method modified with a dynamic flow, a larger-area perovskite crystal film was achieved successfully relying on refreshing the precursor solution and extending the subsequent growth period.

In addition to providing a constantly flowing precursor solution, it is equally effective to accelerate the precursor ions diffusion rate by altering the wettability of substrates that construct the confined space. To promote precursor ions diffusion, Chen et al. developed a hydrophobic interface confined lateral crystal growth method [18]. As shown in Fig. 5(a), at low ions diffusion speed, the precursor consumed by crystal growth is hard to be replenished in time, and the continuous crystal growth process would be interrupted. Meanwhile, random nucleation occurred in the supersaturated region, which would lead to the formation of many small crystals instead of a few crystals with large size. After surface modification, the dramatically enhanced ions diffusion rate could be clearly observed in Fig. 5(b). Compared with that on the hydrophilic surface (glass), the ions diffusion rate is at least 100-fold faster on the hydrophobic surface (poly(bis(4-phenyl)(2,4,6-trimethylphenyl)amine) (PTAA)-covered ITO substrates). This can be attributed to the fact that the nonwetting surface weakens the solvent–substrate interaction, which would promote the diffusion of the solvent. Therefore, the precursor ions would not be dragged during the diffusion, which can accelerate the transportation of precursor ions and then enable the continuous growth of perovskite crystal film to a large area [25]. In a word, when the hydrophilic surface is replaced by the hydrophobic surface, the continuous growth of perovskite crystal films can be achieved. Moreover, the diffusion facilitated space-confined method is universally applicable to both iodide- and bromide- based perovskites. Figures 5(c) and 5(d) show the as-grown $MAPbI_3$ and $MAPbBr_3$ single crystals with millimeter size and 10–20 μm thick.

To conclude, two main strategies are introduced here to accelerate the diffusion rate of precursor ions in the confined space and thus further enlarge the film size. The first one is to introduce the flowing precursor solution into the confined space to increase the diffusion rate of precursor ions. And the other is altering the wettability of substrates from hydrophilic to hydrophobic. Both of these strategies increase the size of perovskite crystal films effectively.

For the size enlargement of perovskite crystal films based on the space-confined method, the strategies mentioned above can be divided into two categories: nucleation control and continuous growth. For the nucleation control, the pre-prepared seed is helpful to suppress random nucleation, and the large size perovskite crystal thin film can be obtained. Moreover, the perovskite array can be achieved according to the orderly arrangement of seed crystals. Besides, through the surface treatment of the substrate in the space-confined method, the nucleation barrier can be adjusted, which can achieve selective nucleation and growth on the target substrate. For the continuous growth of the crystal, the dynamic flow of the precursor solution in a confined space can be realized by a peristaltic pump, which effectively overcomes the difficulty of the insufficient supply of precursor ions. However, this method may increase the preparation complexity, for example, the influence of the dynamic flow rate on the growth and the sealing of the growth module

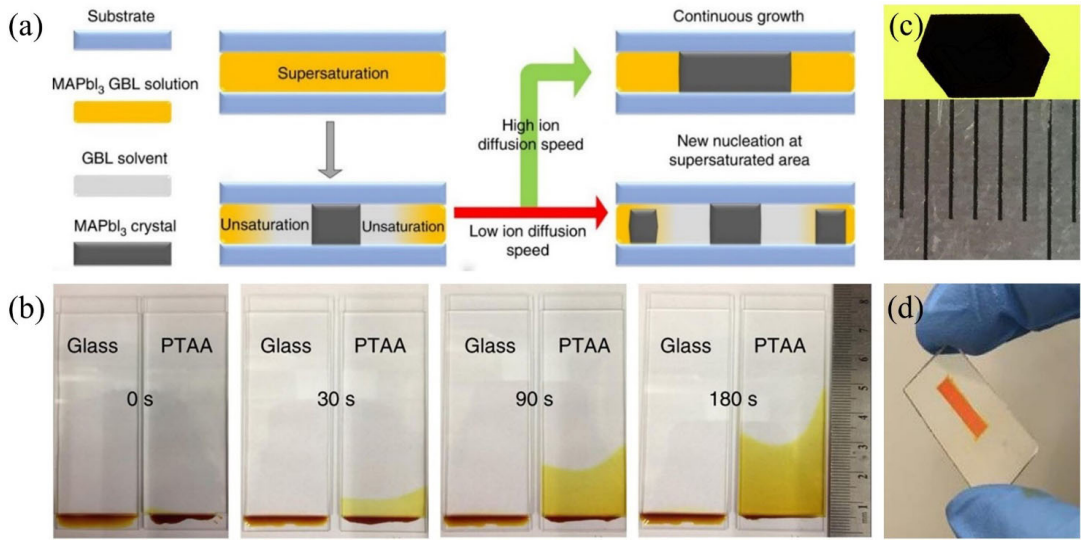


**Figure 5** The space-confined method modified with selective wettability of substrates. (a) Schematic illustration of the correlation between ion diffusion and thin single-crystal growth. (b) Comparison of precursor solution diffusion process using hydrophilic glass and hydrophobic PTAA substrate respectively. Photographs of (c) $MAPbI_3$ and (d) $MAPbBr_3$ thin single crystal using hydrophobic substrates. Reproduced with permission from Ref. [18], © Chen, Z. L. et al. 2017.

needs to be taken into account seriously. Altering the wettability of the substrate in the confined space also helps to increase the size of the perovskite crystal film. Thanks to a relatively hydrophobic surface, the diffusion of the solvent can be promoted, and the continuous growth of large-area films can be realized.

### 3.3 Quality improvement of perovskite crystal films

High quality, which plays a crucial role in determining the electronic properties and the performance of electronic devices, is a desired characteristic of perovskite crystal films. The poor quality of perovskite crystal films is typically expressed as poor crystallinity and small grain size. And they were ascribed to the quick reaction and crystallization of these perovskite materials [36]. Improving crystallinity and size of the grain domains can be expected to reduce the grain boundaries and overall defect density, suppressing carrier recombination during optoelectronic operation. Therefore, the quality improvement of perovskite crystal films has received much attention in this field. Here, recent efforts focused on improving the film quality based on the space-confined method would be presented.

#### 3.3.1 *Crystallization rate control*

Typically, solution-processed perovskite thin films are fabricated via evaporation of the solvent in an open circumstance. However, direct removal of dimethyl sulfoxide (DMSO) or other solvents would severely degrade their quality. For achieving their high-quality preparation, a relatively sealed condition is a reasonable choice to retard the evaporation rate of solvents and improve the crystal quality. The space-confined method is inherently capable of limiting the evaporation of solvents (Fig. 6(a)), just meeting the requirements of high-quality preparation.

As the precursor solutions were confined between two substrates, the solvent could only volatilize through the edge of substrates, which significantly delayed the evaporation rate of the solvent. The slow evaporation rate is favorable to nucleation and subsequent growth of perovskite crystal films [37]. However, in a typical confined space, the solvent evaporation rate at the edge was different from the inside, and the uniformity of crystallization would be affected. Assisted with the unique structure of polydimethylsiloxane (PDMS), Huang et al. realized the slow as well as uniform evaporation of solvent based on the space-confined method, which effectively improved the quality of perovskite crystal films [38]. The PDMS-assisted solvent evaporation crystallization method is described in Fig. 6(b). The PDMS, as a cover, constructes a confined space where the growth rate is well controlled. The high quality of obtained perovskite film was characterized in three aspects: crystallinity, phase purity and surface defects. From single-crystal X-ray diffraction (XRD) measurement (Fig. 6(c)), the strong and sharp diffraction pattern indicates the high quality of the single crystal. The relatively pure phase could be assigned to the uniformly distributed signal from the confocal laser scanning fluorescence picture (Fig. 6(d)). Meanwhile, the trap density of $2.16 \times 10^{13}$ $cm^{-3}$ from the *J*–*V* curve was also obtained to prove the high quality of perovskite single-crystal film, in contrast to the polycrystalline counterpart with the trap density around $4 \times 10^{15}$ $cm^{-3}$ [39]. The improved quality could be attributed to the inherent high porosity of PDMS that equalizes the evaporation rate of the solvent. Besides, due to its non-wettability and flexibility, PDMS can be easily torn from perovskite crystal films, and thus the surface is protected from mechanical damage, which is beneficial to the fabrication of efficient perovskite crystal film solar cells.

#### 3.3.2 *Solvent engineering*

Based on the concept of controlling the solubility of precursor, the evaporation rate of solvent and the supersaturation of solution, the solvent-engineering method is demonstrated as a promising approach to prepare high-quality perovskite crystal films [40, 41]. However, to obtain high-quality perovskite crystal films, most reported crystallization processes usually require considerable time. For example, it can take a few days for solvent evaporation and solution cooling methods [42], or even weeks for the layered solution growth method [43–45].

Considering both the efficiency and quality of preparation, an anti-solvent vapor-assisted method was introduced into the space-confined method: anti-solvent vapor-assisted capping crystallization (AVCC) [46]. It took merely 30 min to synthesize thin $(C_6H_5C_2H_4NH_3)_2PbI_4$ (PEPI) single-crystal films. The anti-solvent vapor-assisted method afforded to grow well defined, rectangle-shaped crystals with lateral size up to centimeter-level and thickness down to micron level. It led to the first rapid and efficient crystallization method for growing large and thin

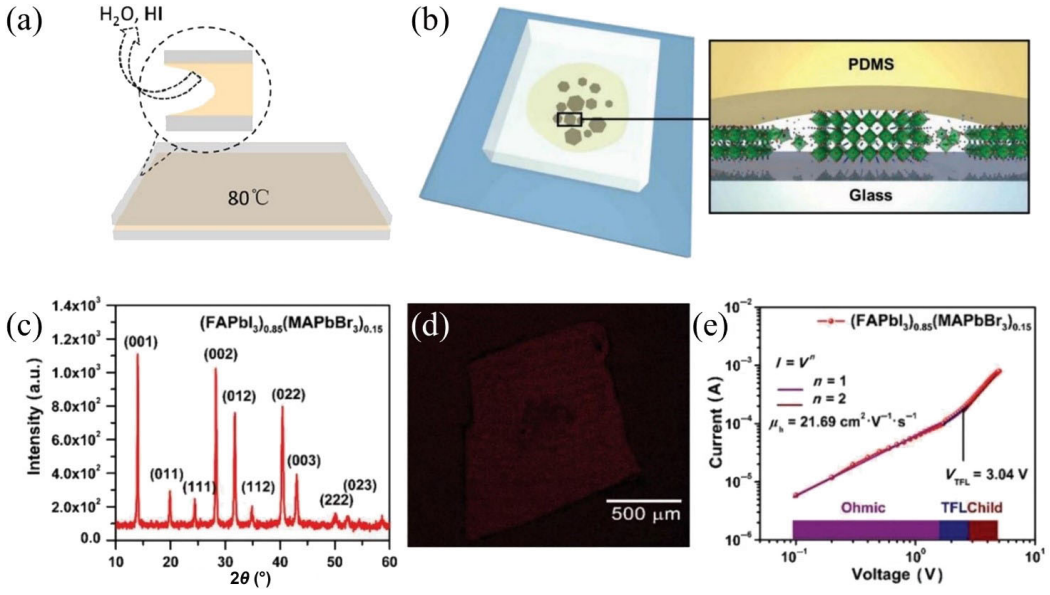


**Figure 6** The space-confined method with the evaporation rate control of solvent. (a) The solvent volatilized through the edge of substrates. Reproduced with permission from Ref. [37], © American Chemical Society 2019. (b) A confined space constructed by PDMS and glass. (c) The powder XRD patterns. (d) The confocal laser scanning fluorescence picture. (e) The *J*–*V* curve of the device. Reproduced with permission from Ref. [38], © WILEY-VCH Verlag GmbH & Co. KGaA, Weinheim 2018.

perovskite single-crystal films. The efficient preparation of high-quality perovskite films can be attributed to the applying of antisolvent. The antisolvent vapor diffused into the precursor solution and then enlarged the local solution concentration, facilitating the nucleation process. Meanwhile, the delayed evaporation of the solution derived from the confined space, leading to the formation of high-quality $CsPbCl_3$ film.

Besides, for the crystallization of perovskite, the choice of solvent used in the synthesis process needs to be taken seriously. In the anti-solvent assisted method, γ-butyrolactone (GBL) was used as the solvent and dichloromethane (DCM) as the antisolvent. Meanwhile, *N*,*N*-dimethylformamide (DMF) is a common solvent for PEPI [47–49]. Therefore, DMF was selected as the solvent for comparison. Figures 7(b) and 7(c) display optical images of growth results using DMF or GBL as solvent by the conventional method. Obviously, compared to DMF, GBL allows a much better crystallization of PEPI and is more suitable for the growth of PEPI. To understand the mechanism of the growth process, the absorption spectra of PEPI precursors dissolved in DMF, GBL and two solvent mixtures were measured respectively. With the increase of GBL content, $PbI_2$ gradually transforms into $[PbI_3]^-$, which may derive from the stronger polarity of GBL than DMF and the strong polarity can better stabilize the charged complexes. To form perovskite, $PbI_2$ has to break apart beforehand and that requires extra energy, whereas $[PbI_3]^-$ is readily available for perovskite formation. Less energy expenditure allows the growth of high-quality PEPI single crystals in GBL rather than in DMF, which accounts for the efficiency of GBL for the crystallization.

In addition to creating an anti-solvent atmosphere to improve the quality of crystals, the antisolvent could be also implemented in the secondary growth process of perovskite crystal films to improve the quality. A pressure-assisted space-confined solvent-engineering strategy (PSS) was designed to dominate the secondary growth of perovskite grains in the films [50], and the procedure of this method is illustrated in Fig. 7(e). The process mainly included three steps: (1) The poor solvent (isopropanol, IPA) droplets were adsorbed on the precursor film by vapor fumigation. (2) As the temperature and pressure rose, the partial crystals were dissolved and the solution diffused in such a relatively sealed circumstance. (3) The fusion and the recrystallization between adjacent crystal grains were conducted. By the way, the antisolvent should be selected carefully. On the premise of dissolving small crystal grains without damaging large crystal grains, both low boiling point and poor solubility for precursors are necessary. In the whole process, the method combines the effects of pressure assistance, space confinement and solvent engineering to form the high-quality $MAPbI_3$ film. Compared to the conventional annealing (CA) process, the XRD pattern of the film grown by the PSS approach shows sharper and stronger perovskite (110) and (220) peaks (Fig. 7(f)), which indicates the improved crystallinity of the $MAPbI_3$. The large grain size and the fusion between adjacent grains are illustrated by scanning electron microscopy (SEM) results (Figs. 7(g) and 7(h)). Above all, the annealing of antisolvent does have a significant effect on the quality of perovskite films, including crystallinity, grain size and grain boundary [51]. The key point in PSS approaches is the adsorption of poor solvent in the preheating film. As pressure and temperature increase, partial perovskite crystal grains with small size and poor crystallinity would be dissolved by IPA. And the wet atmosphere could facilitate the diffusion of dissolved precursors to support the further growth of perovskite crystal grains with large size. So, the grain size and crystallinity can be improved via such a dissolution-recrystallization process. Meanwhile, the quick removal of the solvent is prevented from the relatively sealed circumstance and the period that solvent stayed with the film is prolonged, which allows a repeated crystallization-dissolution-crystallization process to continually repair the film. Thus, the film with large crystalline grains can be yield.

To conclude, slowing down the rate of solvent evaporation and crystallization process through a relatively sealed space or an atmosphere of anti-solvent, as well as the recrystallization in secondary growth induced by weak solvent can effectively improve the quality of perovskite crystal films.

For the quality improvement of perovskite crystal films base on the space-confined method, slowing down the crystallization process by controlling the evaporation rate of the solvent is a major feature to obtain high-quality crystals. However, the

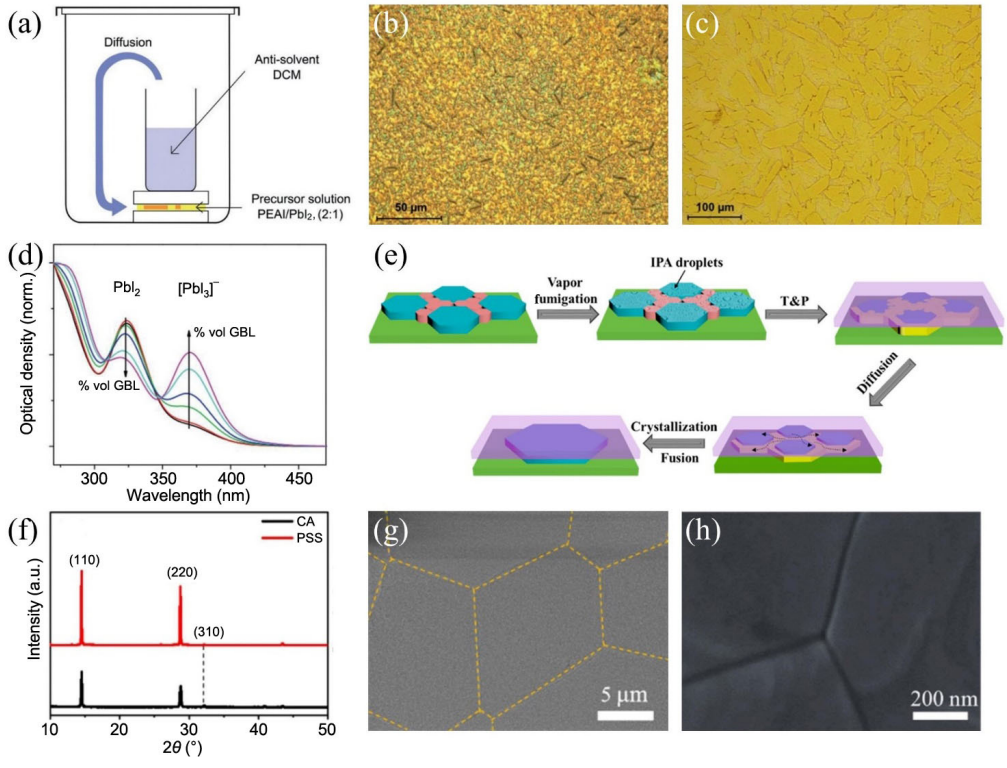


**Figure 7** The space-confined method modified with poor solvent. (a) Schematic diagram of the AVCC process. Optical images of PEPI thin films using (b) DCM and (c) GBL as the solvent. (d) Absorption spectra of precursor solutions in DMF with an increasing amount of GBL. Reproduced with permission from Ref. [46], © The Royal Society of Chemistry 2017. (e) The growth process of the $MAPbI_3$ film by the PSS strategy. (f) XRD patterns of the CA and PSS $MAPbI_3$ films. (g) Magnification SEM image of the PSS film. (h) SEM image of the triple junction of grain boundaries. Reproduced with permission from Ref. [50], © American Chemical Society 2018.

uniformity of crystallization is affected by the difference of evaporation rate between the edge and center of the liquid layer in confined space. Using porous PDMS as the substrate can realize the slow and uniform evaporation of the solvent, which is helpful for the preparation of high-quality crystals. Also, considering the preparation efficiency, the combination of the antisolvent method and the space-confined method is an effective strategy to ensure both preparation efficiency and crystal quality. Besides, for avoiding grain boundaries and small grains that commonly occurred during the crystal growth process, the introduction of weak solvent-induced recrystallization is a suitable strategy.

### 3.4 Architecture tailoring of perovskite crystal films

Above mentioned strategies via space-confined methods are based on the limited space constructed by two flat substrates, and the corresponding product is also presented in a form of planar thin film. However, the architecture of perovskites also plays a vital role in the performance of photoelectric devices [52]. For instance, perovskite materials with various structures, such as nanowires [53–55], nanoislands [56] and inverse opals [57], have been fabricated through morphology control. Compared with their flat film counterpart, these nanostructured and microstructured perovskite materials exhibit high photosensitivity owing to unique architecture with a large surface-to-volume ratio that is beneficial to light absorption and charge collection [52].

In this regard, a space-confined growth modified with ordered polystyrene (PS) sphere template was reported [58]. The fabrication process of the $CsPbBr_3$ nanonet film is schematically illustrated in Fig. 8(b). The resulting $CsPbBr_3$ nanonet film shows a homogeneous surface and closely packed large crystal grains (Fig. 8(b4)), which is favorable for practical applications. For comparison, a conventional spin-coating process was used to prepare $CsPbBr_3$ films as shown in Fig. 8(a). Since the low solubility of precursors and the fast growth rate, the conventional $CsPbBr_3$ film shows a discontinuous surface and lots of grain boundaries, which can be observed in Fig. 8(a4). Consequently, thanks to the restricted narrow growth space provided by PS templates, the evaporation of the solvent can be delayed and the fast crystallization process is alleviated. As a result, ultradense $CsPbBr_3$ nanonet film with preferred orientation and enlarged crystal grains can be achieved, which exhibits the low trap-state density ($3.07 \times 10^{12}$ $cm^{-3}$) and high carrier mobility (9.27 $cm^2 \cdot V^{-1} \cdot s^{-1}$). Furthermore, endowed by the net-like structure, the utilization efficiency of raw materials and light-harvesting ability are enhanced significantly as enlargement of limited area. Benefitting from both excellent properties and high absorption coefficient, photodetectors based on these films exhibit high performance, including a high responsivity of 216 $A \cdot W^{-1}$ and a short ultraresponse time within 5 μs.

Based on a similar method, Liu et al. altered the diameter of PS spheres, and the nanonet films with various sizes nanoholes were prepared to optimize the orientation of the crystal [59]. Generally, the perovskite films prepared by the conventional one-step spin-coating method exhibit a preferred orientation in the (100) direction [60, 61]. Yet the orientation is undesired for device performance. For instance, the photodetectors based on the (110) and (112) plane-oriented perovskites were reported respectively, and show an enhancement of responsivity and photocurrent compared to that of the device based on perovskites with the (100) orientation [52, 62]. These results suggest that suppressing the (100) orientation of perovskite films may provide an effective way to realize better device performance. In this method, based on the monolayer nano-PS confined growth, with the increase of spherical diameter, the (100) orientation

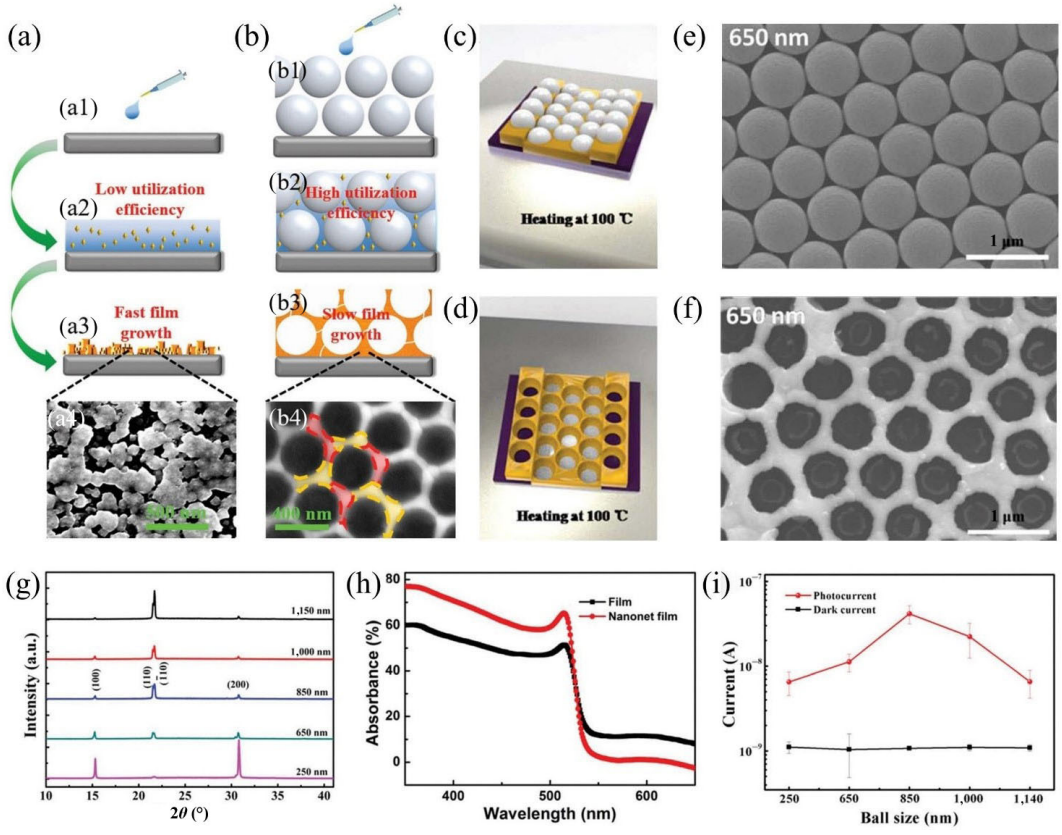


**Figure 8** Schematic illustration of (a) conventional and (b) space-confined $CsPbBr_3$ film fabrication strategies. Reproduced with permission from Ref. [58], © WILEY-VCH Verlag GmbH & Co. KGaA, Weinheim 2018. Schematic illustration of PS spheres (c) and the $CsPbBr_3$ prepared with PS spheres (d) in the synthesis process of the $CsPbBr_3$ nanonet films. Top SEM images of the PS spheres (e) and the $CsPbBr_3$ prepared with PS spheres (f), the diameter of PS spheres is 650 nm. (g) XRD patterns of the $CsPbBr_3$ nanonet films with various nanoholes. (h) Absorption characteristic of the conventional spin-coated $CsPbBr_3$ film and $CsPbBr_3$ nanonet film. (i) Dark- and photo-current of the $CsPbBr_3$ nanonet films prepared with various PS spheres. Reproduced with permission from Ref. [59], © The Royal Society of Chemistry 2019.

is inhibited, while the degree of preferred orientation on the (110) plane of $CsPbBr_3$ nanonet films increases. The PS templates with various sizes spheres range from 250 to 1,150 nm. Among them, 850 nm is regarded as the most appropriate diameter of PS spheres which leads to the best performance in photodetectors.

In addition, assisted with nanoimprinting techniques or phase transformation, more periodic nanostructures (patterned thin films) have been also prepared in the confined space. For the space-confined method modified with phase transformation, the as-prepared perovskite film transformed from solid to liquid in methylamine (MA) gas atmosphere, and then from liquid to solid in annealing [63]. Through perovskite recrystallization during phase transformation, the planar film was successfully converted into periodic nanostructures with the presence of a periodic mold. This method realized both periodically nanostructured and well-crystallized perovskites, which offers better photoelectric properties than their flat film counterparts. What's more, for the space-confined method modified with nanoimprinting techniques, as shown in Fig. 9(d), a patterned rolling mold is used to confine lateral crystal growth of perovskite ink solution [64]. The concept of this printing method is universal and could be expanded to fabricate various materials such as semiconductor and polymer materials.

For the architecture tailoring of perovskite crystal films based on the space-confined method, the unique architecture, like net-like structure or periodic structure, endows perovskite thin films with a large surface to volume ratio, which is beneficial to light absorption and charge collection, thus improving the device performance. However, because of this special discontinuous structure, grain boundaries are prone to appear and affect the crystal quality. Thus, in the growth process of perovskite nanonet films through the space-confined growth modified with ordered PS template, some factors need to be optimized, such as the size and the stacked layers of PS spheres. And, for the space-confined method modified with nanoimprinting techniques, the moving speed of the patterned rolling mold needs to be carefully controlled to avoid too fast crystallization rate.

### 3.5 Others

Apart from the optimization of thickness, size, quality and architecture, there are more possibilities for the space-confined method to further improve perovskite crystal films. Here, stability investigating and component regulating are discussed briefly. Specifically, the mechanism of stabilization was investigated by studying ions migration in the perovskite crystal film prepared by the space-confined method. Moreover, a halogen gradient can be obtained by adjusting the halogen distribution through a gaseous halide exchange process to improve the photoelectric performance of perovskite crystal films prepared by the space-confined method.

#### 3.5.1 *Stability investigating*

At present, the major hindrance to the commercialization of perovskite solar cells is its instability compared to their silicon counterparts. In particular, there are two main sources of relatively low stability. One is the reactivity of perovskite crystals with environmental factors, including moisture, oxygen, heat,

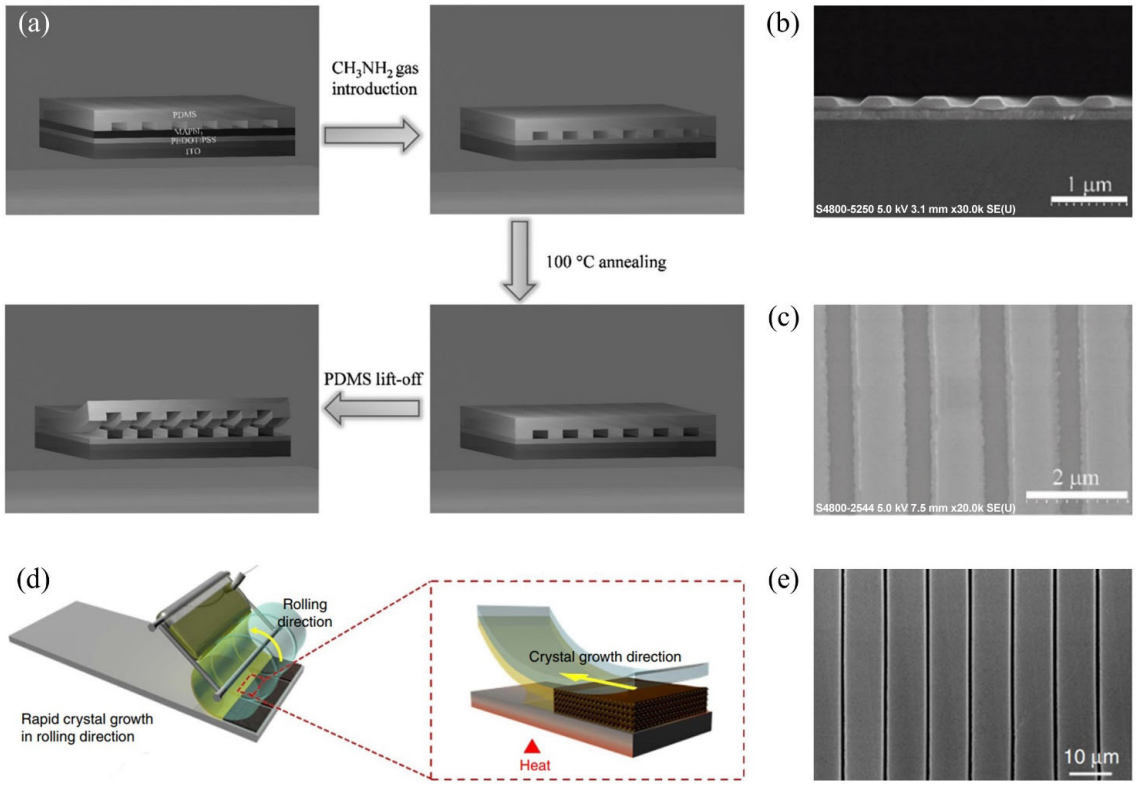


**Figure 9** The space-confined method modified with patterned substrates. (a) The fabrication process of perovskite periodic nanostructures through phase transformation. (b) and (c) Cross-sectional and top-view SEM image. Reproduced with permission from Ref. [63], © WILEY-VCH Verlag GmbH & Co. KGaA, Weinheim 2017. (d) Schematic of the manufacturing procedure for single-crystal perovskite thin films using geometrically confined lateral crystal growth with a rolling mold. (e) Top-view SEM image of single-crystal perovskite patterned thin film. Reproduced with permission from Ref. [64], © Springer Nature 2017.

as well as ultraviolet light [65–67]. The other issue is the internal intrinsic ion diffusion-induced corrosion of perovskite [68, 69]. To date, most of the external stimuli can be negated by sophisticated device encapsulation or other strategies [70, 71]. While the internal issue needs more attention to further enhance the stability of perovskite solar cells [72].

Based on the space-confined method with modified substrate wettability that mentioned earlier, Xiao et al. obtained a large-area quasi-2D perovskite thin single-crystal film, which has a typical lateral size of 4 mm and a thickness of 20 μm [25]. Compared with 3D perovskite, the group found that the quasi-2D perovskite prepared by the space-confined method exhibited better stability. On this basis, the ion migration in perovskite that affects the stability was further studied. The temperature-dependent conductivity results indicate that the ion migration along the in-plane direction is suppressed in the quasi-2D perovskite. Normally, in the low-temperature region, electronic conductivity is responsible for the material conductivity, while the ionic conductivity plays a leading role in the high-temperature region. The measurements for the conductivity of 3D and quasi-2D single-crystal perovskites at varied temperatures are presented in Figs. 10(b) and 10(c),

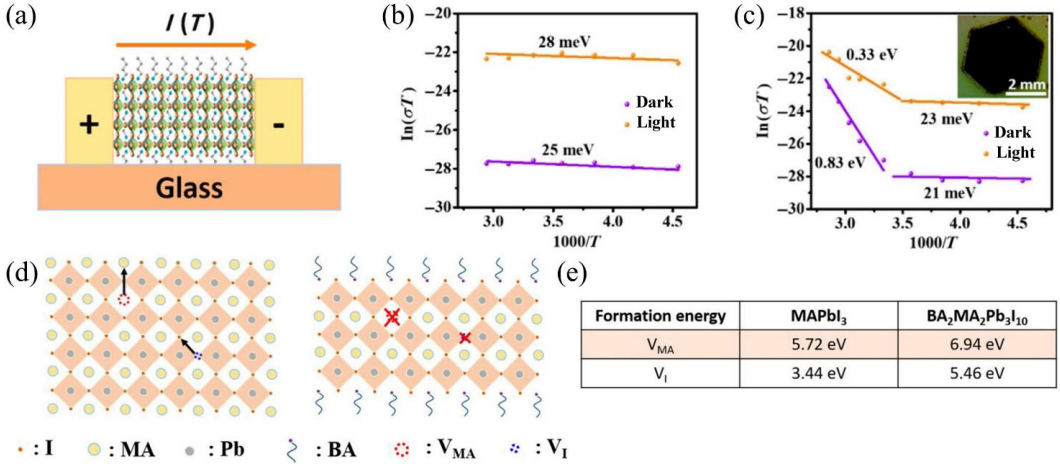


(e)

| Formation energy | $MAPbI_3$ | $BA_2MA_2Pb_3I_{10}$ |
|---|---|---|
| $V_{MA}$ | 5.72 eV | 6.94 eV |
| $V_I$ | 3.44 eV | 5.46 eV |

**Figure 10** The ion migration in perovskite crystal films. (a) Scheme for the in-plane temperature-dependent conductivity of a quasi-2D perovskite. (b) and (c) Results of temperature-dependent conductivity measurement of 3D $MAPbI_3$ and quasi-2D $BA_2MA_2Pb_3I_{10}$ perovskite single-crystal films, respectively. (d) Schemes of vacancy path for ion migration and (e) formation energy of vacancy defects in 3D and quasi-2D perovskites. Reproduced with permission from Ref. [25], © American Chemical Society 2018.

respectively. It can be found that ion migration is obviously inhibited in quasi-two-dimensional perovskite. Since grain boundaries are not available in quasi-2D single crystals, the ion migration has to depend on the vacancy. Therefore, the researchers calculated the formation energy of vacancy by density functional theory (DFT) calculation, and the results show that the formation energy of vacancy in quasi-2D perovskite is higher than that in 3D one. The increase of vacancy formation energy in quasi-2D perovskites, results in the reduction of vacancy and absence of ion migration, which effectively enhances the efficiency and stability of perovskite-based electronic devices.

To conclude, owing to the absence of grain boundaries in single crystals as well as the increased vacancy formation energy in quasi-2D perovskites, the ion diffusion is dramatically suppressed and thus the stability of perovskite can be significantly enhanced.

### 3.5.2 *Components regulating*

The performance of fabricated optoelectronic devices can be affected by the carrier loss in perovskite. To reduce the recombination of carriers, the thickness reduction discussed earlier is a quite good strategy. However, the perovskite single crystals with an ultra-thin thickness (< 1 μm) typically possess a relatively small area (< 1 $mm^2$), which is still not suitable for practical applications [11, 24]. Recently, halide gradient perovskite films have been found to enhance the hole transportation and then improve the photoelectric performance via forming a built-in electric field [73, 74].

After the perovskite film was prepared by the space-confined method, it could be converted into halide gradient perovskite film to further improve the performance of photoelectric devices. A facile conversion method was reported by Li et al. Based on their previous work of growing perovskite by the space-confined method [35], they prepared halide gradient perovskite films by a space-limited inverse temperature crystallization growth method and a subsequent gaseous halide exchange process [75]. The gas-solid exchange process is illustrated in Fig. 11(a), and the color change in optical image (Figs. 11(b) and 11(c)) indicates the conversion from $MAPbBr_3$ single crystal to $MAPbBr_3/MAPbBr_{3-x}I_x$ graded heterojunction single crystal (GHSC). Such a halide gradient distribution would enable efficient carrier separation and retard recombination significantly. Accordingly, a photodetector based on it displays a high external quantum efficiency (EQE) (170% at 2 V) and short response time (0.56 ms). In the EQE spectra (Fig. 11(d)), compared with 100 μm thick $MAPbBr_3$ crystal film (20% and 80% at 1 and 2 V bias), the as-prepared 11 μm thick pure laminar $MAPbBr_3$ device exhibits a higher EQE (25% and 120% at 0 and 2 V bias) due to the reduced thickness. Furthermore, much higher EQE (40% and 170% at 0 and 2 V bias) is achieved with the $MAPbBr_3/MAPbBr_{3-x}I_x$ GHSC, which is attributed to the halide gradient heterojunction. Then the potential profile across the halide gradient region was measured by Kelvin probe force microscopy. The gradually reduced potential along a gradient distribution of the iodine element indicates the existence of a built-in electric field, which is the key to accelerate carrier transport and suppress recombination loss for the enhancement of device performance. And shorter carrier transport time and longer carrier lifetime were further confirmed by the transient photocurrent and photovoltage measurements.

In a word, from thickness reduction achieved by the

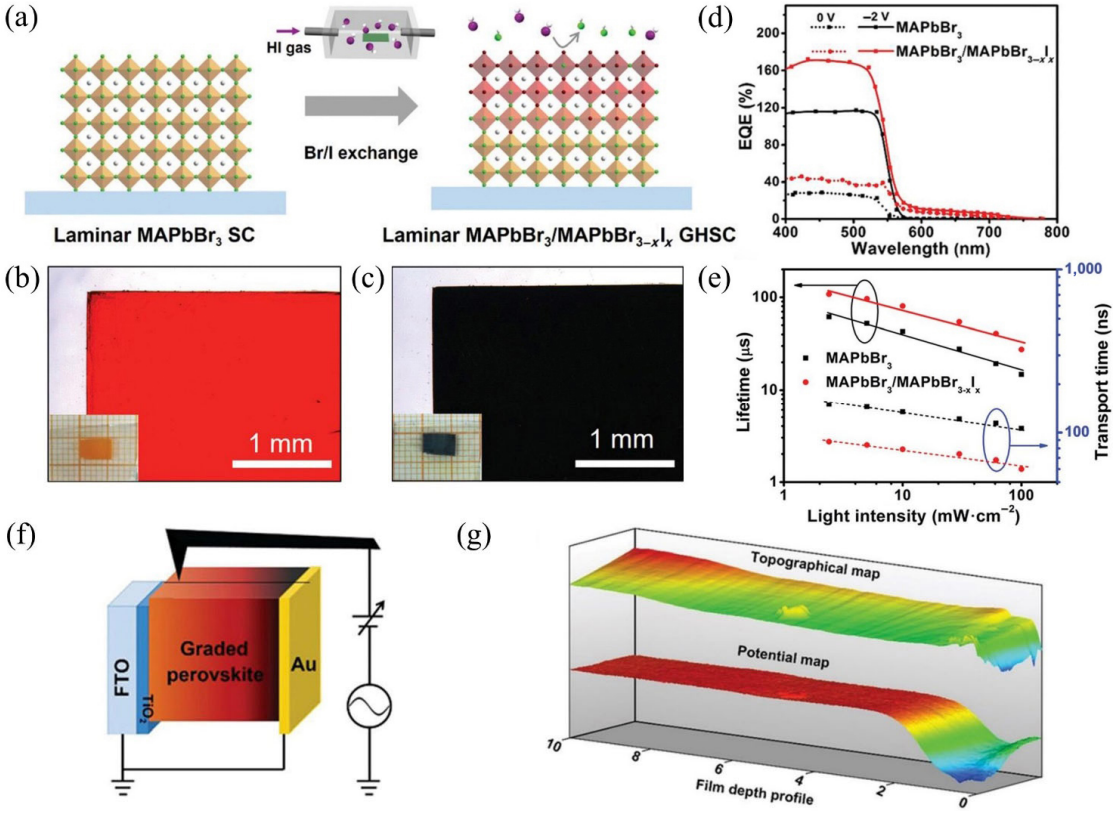


**Figure 11** The conversion from $MAPbBr_3$ single crystal film to $MAPbBr_3/MAPbBr_{3-x}I_x$ GHSC film. (a) Schematic illustration of the laminar $MAPbBr_3/MAPbBr_{3-x}I_x$ GHSC prepared via a post gaseous halide exchange process. The optical images of (b) the laminar $MAPbBr_3$ single crystal film and (c) $MAPbBr_3/MAPbBr_{3-x}I_x$ GHSC film. The performance of photodetectors based on the $MAPbBr_3$ and $MAPbBr_3/MAPbBr_{3-x}I_x$: (d) the recombination lifetimes and transport times and (e) EQE spectra. (f) Schematic of the cross-sectional KPFM measurement setup. (g) The topography and the corresponding surface potential mapping across the halide gradient region. Reproduced with permission from Ref. [75], © The Royal Society of Chemistry 2019.

space-confined method to halide gradient heterojunction by a post gaseous halide exchange process, the device performance could be further improved significantly.

## 4 Device performance

The performance of photodetectors based on the space-confined perovskite crystal films is summarized in Table 1. The excellent optical and charge-transport properties of perovskite have enabled their successful development in photoelectric devices. Here, taking the photodetector as an example, the correlation between the thickness of the perovskite crystal film and the device performance is investigated. For photodetectors, the thickness of perovskite plays a crucial role in device performance. Generally, the device performance of photodetectors based on perovskite films tends to be enhanced as the thickness decreases. For example, based on the space-confined method, Ma et al. prepared a perovskite film with a thickness of 380 nm, and the corresponding photodetector exhibits a high responsivity of $10^1$–$10^7$ A·W$^{-1}$ at −1.5 V bias [11]. Compared to the previously reported responsivity in perovskite photodetectors with a millimeter or submillimeter thickness (0.02 A·W$^{-1}$ at a −1 V bias for 2 mm-thick $MAPbBr_3$; 2 mA·W$^{-1}$ at a 0 V bias for 150 μm-thick $MAPbBr_3$), such a high responsivity is higher than those similar photodetectors [76, 77]. (And for a thinner one, the perovskite film with 20 nm, prepared through the space-confined method by Wang et al., the corresponding response time is reduced). Specifically, the rise time and decay time are 5 and 4.1 μs, respectively, much faster than their thicker counterpart [78]. In the work of Kuang et al., the thickness of perovskite films ranged from 100 to 800 μm, and the corresponding response time of the photoelectric detector is extended from 120 to 2,710 μs, showing a reduced photoresponsivity [28]. The charge recombination caused by an excess thickness is responsible for the degradation of device performance. In particular, although the optoelectronic responsivity decreases with thickness, the response spectrum changed from broadband to narrowband with the increase of thickness, which is beneficial for narrowband detection. Therefore, for the improvement of device performance, the appropriate thickness is needed for device construction according to the actual detection requirements. Also, it demonstrates the significance of thickness control in the space-confined method introduced in this paper. Besides, the optimization of device performance is not only limited to the thickness of perovskite film. Benefiting from enlarged surface to volume ratio and the gradient distribution of the halogens respectively, tailoring the architecture of perovskite crystal films through the space-confined method and further composition regulating are all conducive to the device with better performance.

## 5 Conclusions and perspective

In summary, the space-confined method is a facile and effective way for the controllable preparation of perovskite crystal films. With applying appropriate modified strategies, various widely concerned issues of perovskite preparation can be effectively alleviated, including thickness adjustment, size enlargement, quality improvement and architecture tailoring of perovskite crystal films. These improvements satisfy a majority of requirements of high-performance photoelectric devices well. Even though lots of progress has been achieved by the space-confined method, there are still some concerns that need to be addressed. For example, most of the space-confined methods are based on the liquid phase, and the perovskites grown in solution generally possess a large number of surface charge traps, which will lead to unsatisfactory performance. So, rational surface passivation strategies need to be further developed. Moreover, substrate-independent growth is a characteristic of the space-confined method, which is favorable for developing highly integrated systems and reducing device fabrication complexity. However, the lattice mismatch between perovskite and substrate may degrade the device performance, thus the selection of substrates should be considered carefully in advance. Finally, considering the instability of the volatile organic component and toxicity of the lead element in perovskite, all-inorganic and lead-free perovskite should be realized by a further modified method. All in all, based on the space-confined method, simple and flexible fabrication of perovskite crystal thin films with controlled thickness, enlarged size, improved quality and tailored architecture will definitely make perovskite an excellent alternative material for photovoltaic applications in the coming future.

**Table 1** Summary of the performance of photodetectors based on the space-confined perovskite crystal films

| Material | Thickness (μm) | Structure | Responsivity (A·W$^{-1}$) | EQE (%) | Response time (μs) | Test condition | Ref. |
|---|---|---|---|---|---|---|---|
| $MAPbBr_3$ | 0.38 | Vertical type | $10^1$–$10^7$ | — | 88; 930 | −1.5 V bias | [11] |
| $MAPbI_3$ | 35 | Planer type | 5 | — | 39,000; 17,000 | 5 V bias | [26] |
| $MAPbI_3$ | 490 | Planar type | 1–2.5 | 600 | — | 2 V bias | [27] |
| $MAPbBr_3$ | 100 | Vertical type | — | 19.8 | 120 | −1 V bias | [28] |
| $MAPbBr_3$ | 200 | Vertical type | — | 3.79 | 350 | −1 V bias | [28] |
| $MAPbBr_3$ | 400 | Vertical type | — | 0.6 | 1140 | −1 V bias | [28] |
| $MAPbBr_3$ | 800 | Vertical type | — | 0.004 | 2710 | −1 V bias | [28] |
| $MAPbI_3$ | 170 | Planer type | 3.87 | 904 | 350; 420 | 1 V bias | [33] |
| $(BA)_2(MA)Pb_2I_7$ | 0.18 | Planar type | 2.96 | — | 4000 | 1 V bias | [37] |
| $MAPbI_3$ | 0.5 | Planar type | — | — | 23; 30 | 10 V bias | [50] |
| $CsPbBr_3$ (nanonet) | 0.66 | Planer type | 216 | 37.04 | 3.96; 4.92 | 1 V bias | [58] |
| $CsPbBr_3$ (nanonet) | 0.57 | Vertical type | 2.84 | — | 11,000; 16,000 | 5 V bias | [59] |
| $MAPbBr_3/MAPbBr_{3-x}I_x$ | 11 | Vertical type | — | 170 | 0.56 | −2 V bias | [75] |
| $MAPbBr_3$ | 11 | Vertical type | — | 120 | 0.67 | −2 V bias | [75] |
| $MAPbBr_3$ | 0.02 | Planer type | 126 | — | 5; 4.1 | 5 V bias | [78] |
| $CsPbCl_3$ | 0.5 | Planer type | 0.45 | — | 8,000; 7,000 | 5 V bias | [79] |

## Acknowledgements

This work was supported by the National Natural Science Foundation of China (Nos. 21673161 and 21905210), the Sino-German Center for Research Promotion (1400), and the Postdoctoral Innovation Talent Support Program of China (No. BX20180224).

## References

[1] Ogomi, Y.; Morita, A.; Tsukamoto, S.; Saitho, T.; Fujikawa, N.; Shen, Q.; Toyoda, T.; Yoshino, K. J.; Pandey, S. S.; Ma, T. L. et al. $CH_3NH_3Sn_xPb_{(1-x)}I_3$ perovskite solar cells covering up to 1,060 nm. *J. Phys. Chem. Lett.* **2014**, *5*, 1004–1011.

[2] Kazim, S.; Nazeeruddin, M. K.; Grätzel, M.; Ahmad, S. Perovskite as light harvester: A game changer in photovoltaics. *Angew. Chem., Int. Ed.* **2014**, *53*, 2812–2824.

[3] Dong, Q. F.; Fang, Y. J.; Shao, Y. C.; Mulligan, P.; Qiu, J.; Cao, L.; Huang, J. S. Electron-hole diffusion lengths >175 μm in solution-grown $CH_3NH_3PbI_3$ single crystals. *Science* **2015**, *347*, 967–970.

[4] Xu, H.; Chen, R. F.; Sun, Q.; Lai, W. Y.; Su, Q. Q.; Huang, W.; Liu, X. G. Recent progress in metal-organic complexes for optoelectronic applications. *Chem. Soc. Rev.* **2014**, *43*, 3259–3302.

[5] Sum, T. C.; Mathews, N. Advancements in perovskite solar cells: Photophysics behind the photovoltaics. *Energy Environ. Sci.* **2014**, *7*, 2518–2534.

[6] Yang, W. S.; Noh, J. H.; Jeon, N. J.; Kim, Y. C.; Ryu, S.; Seo, J.; Seok, S. I. High-performance photovoltaic perovskite layers fabricated through intramolecular exchange. *Science* **2015**, *348*, 1234–1237.

[7] Bi, D. Q.; Tress, W.; Dar, M. I.; Gao, P.; Luo, J. S.; Renevier, C.; Schenk, K.; Abate, A.; Giordano, F.; Correa Baena, J. P. et al. Efficient luminescent solar cells based on tailored mixed-cation perovskites. *Sci. Adv.* **2016**, *2*, e1501170.

[8] Dou, L. T.; Yang, Y.; You, J. B.; Hong, Z. R.; Chang, W. H.; Li, G.; Yang, Y. Solution-processed hybrid perovskite photodetectors with high detectivity. *Nat. Commun.* **2014**, *5*, 5404.

[9] Lv, Q. R.; Lian, Z. P.; He, W. H.; Sun, J. L.; Li, Q.; Yan, Q. F. A universal top-down approach toward thickness-controllable perovskite single-crystalline thin films. *J. Mater. Chem. C* **2018**, *6*, 4464–4470.

[10] Han, L. P.; Liu, C.; Wu, L. L.; Zhang, J. Q. Observation of the growth of $MAPbBr_3$ single-crystalline thin film based on space-limited method. *J. Cryst. Growth* **2018**, *501*, 27–33.

[11] Yang, Z. Q.; Deng, Y. H.; Zhang, X. W.; Wang, S.; Chen, H. Z.; Yang, S.; Khurgin, J.; Fang, N. X.; Zhang, X.; Ma, R. M. High-performance single-crystalline perovskite thin-film photodetector. *Adv. Mater.* **2018**, *30*, 1704333.

[12] Peng, W.; Wang, L. F.; Murali, B.; Ho, K. T.; Bera, A.; Cho, N.; Kang, C. F.; Burlakov, V. M.; Pan, J.; Sinatra, L. et al. Solution-grown monocrystalline hybrid perovskite films for hole-transporter-free solar cells. *Adv. Mater.* **2016**, *28*, 3383–3390.

[13] Chen, J.; Morrow, D. J.; Fu, Y. P.; Zheng, W. H.; Zhao, Y. Z.; Dang, L. N.; Stolt, M. J.; Kohler, D. D.; Wang, X. X.; Czech, K. J. et al. Single-crystal thin films of cesium lead bromide perovskite epitaxially grown on metal oxide perovskite ($SrTiO_3$). *J. Am. Chem. Soc.* **2017**, *139*, 13525–13532.

[14] Wang, Y. P.; Sun, X.; Chen, Z. Z.; Sun, Y. Y.; Zhang, S. B.; Lu, T. M.; Wertz, E.; Shi, J. High-temperature ionic epitaxy of halide perovskite thin film and the hidden carrier dynamics. *Adv. Mater.* **2017**, *29*, 1702643.

[15] Liu, Y. C.; Sun, J. K.; Yang, Z.; Yang, D.; Ren, X. D.; Xu, H.; Yang, Z. P.; Liu, S. Z. 20-mm-large single-crystalline formamidinium-perovskite wafer for mass production of integrated photodetectors. *Adv. Opt. Mater.* **2016**, *4*, 1829–1837.

[16] Liu, Y. C.; Ren, X. D.; Zhang, J.; Yang, Z.; Yang, D.; Yu, F. Y.; Sun, J. K.; Zhao, C. M.; Yao, Z.; Wang, B. et al. 120 mm single-crystalline perovskite and wafers: Towards viable applications. *Sci. China Chem.* **2017**, *60*, 1367–1376.

[17] Chen, Z. L.; Turedi, B.; Alsalloum, A. Y.; Yang, C.; Zheng, X. P.; Gereige, I.; AlSaggaf, A.; Mohammed, O. F.; Bakr, O. M. Single-crystal $MAPbI_3$ perovskite solar cells exceeding 21% power conversion efficiency. *ACS Energy Lett.* **2019**, *4*, 1258–1259.

[18] Chen, Z. L.; Dong, Q. F.; Liu, Y.; Bao, C. X.; Fang, Y. J.; Lin, Y.; Tang, S.; Wang, Q.; Xiao, X.; Bai, Y. et al. Thin single crystal perovskite solar cells to harvest below-bandgap light absorption. *Nat. Commun.* **2017**, *8*, 1890.

[19] Wang, X. D.; Li, W. G.; Liao, J. F.; Kuang, D. B. Recent advances in halide perovskite single-crystal thin films: Fabrication methods and optoelectronic applications. *Sol. RRL* **2019**, *3*, 1800294.

[20] Saidaminov, M. I.; Abdelhady, A. L.; Murali, B.; Alarousu, E.; Burlakov, V. M.; Peng, W.; Dursun, I.; Wang, L. F.; He, Y.; Maculan, G. et al. High-quality bulk hybrid perovskite single crystals within minutes by inverse temperature crystallization. *Nat. Commun.* **2015**, *6*, 7586.

[21] Maculan, G.; Sheikh, A. D.; Abdelhady, A. L.; Saidaminov, M. I.; Haque, M. A.; Murali, B.; Alarousu, E.; Mohammed, O. F.; Wu, T.; Bakr, O. M. $CH_3NH_3PbCl_3$ single crystals: Inverse temperature crystallization and visible-blind UV-photodetector. *J. Phys. Chem. Lett.* **2015**, *6*, 3781–3786.

[22] Dang, Y. Y.; Liu, Y.; Sun, Y. X.; Yuan, D. S.; Liu, X. L.; Lu, W. Q.; Liu, G. F.; Xia, H. B.; Tao, X. T. Bulk crystal growth of hybrid perovskite material $CH_3NH_3PbI_3$. *CrystEngComm* **2015**, *17*, 665–670.

[23] Shi, D.; Adinolfi, V.; Comin, R.; Yuan, M. J.; Alarousu, E.; Buin, A.; Chen, Y.; Hoogland, S.; Rothenberger, A.; Katsiev, K. et al. Low trap-state density and long carrier diffusion in organolead trihalide perovskite single crystals. *Science* **2015**, *347*, 519–522.

[24] Chen, Y. X.; Ge, Q. Q.; Shi, Y.; Liu, J.; Xue, D. J.; Ma, J. Y.; Ding, J.; Yan, H. J.; Hu, J. S.; Wan, L. J. General space-confined on-substrate fabrication of thickness-adjustable hybrid perovskite single-crystalline thin films. *J. Am. Chem. Soc.* **2016**, *138*, 16196–16199.

[25] Xiao, X.; Dai, J.; Fang, Y. J.; Zhao, J. J.; Zheng, X. P.; Tang, S.; Rudd, P. N.; Zeng, X. C.; Huang, J. S. Suppressed ion migration along the in-plane direction in layered perovskites. *ACS Energy Lett.* **2018**, *3*, 684–688.

[26] Wang, Q.; Bai, D. L.; Jin, Z. W.; Liu, S. Z. Single-crystalline perovskite wafers with a Cr blocking layer for broad and stable light detection in a harsh environment. *RSC Adv.* **2018**, *8*, 14848–14853.

[27] Liu, Y. C.; Zhang, Y. X.; Yang, Z.; Yang, D.; Ren, X. D.; Pang, L. Q.; Liu, S. Z. Thinness- and shape-controlled growth for ultrathin single-crystalline perovskite wafers for mass production of superior photoelectronic devices. *Adv. Mater.* **2016**, *28*, 9204–9209.

[28] Rao, H. S.; Li, W. G.; Chen, B. X.; Kuang, D. B.; Su, C. Y. *In situ* growth of 120 $cm^2$ $CH_3NH_3PbBr_3$ perovskite crystal film on FTO glass for narrowband-photodetectors. *Adv. Mater.* **2017**, *29*, 1602639.

[29] Yantara, N.; Bhaumik, S.; Yan, F.; Sabba, D.; Dewi, H. A.; Mathews, N.; Boix, P. P.; Demir, H. V.; Mhaisalkar, S. Inorganic halide perovskites for efficient light-emitting diodes. *J. Phys. Chem. Lett.* **2015**, *6*, 4360–4364.

[30] Zhang, H. J.; Liu, X.; Dong, J. P.; Yu, H.; Zhou, C.; Zhang, B. B.; Xu, Y. D.; Jie, W. Q. Centimeter-sized inorganic lead halide perovskite $CsPbBr_3$ crystals grown by an improved solution method. *Cryst. Growth Des.* **2017**, *17*, 6426–6431.

[31] Kim, W.; Jung, M. S.; Lee, S.; Choi, Y. J.; Kim, J. K.; Chai, S. U.; Kim, W.; Choi, D. G.; Ahn, H.; Cho, J. H. et al. Oriented grains with preferred low-angle grain boundaries in halide perovskite films by pressure-induced crystallization. *Adv. Energy Mater.* **2018**, *8*, 1702369.

[32] Yue, H. L.; Sung, H. H.; Chen, F. C. Seeded space-limited crystallization of $CH_3NH_3PbI_3$ single-crystal plates for perovskite solar cells. *Adv. Electron. Mater.* **2018**, *4*, 1700655.

[33] Gao, J.; Liang, Q. B.; Li, G. H.; Ji, T.; Liu, Y. C.; Fan, M. M.; Hao, Y. Y.; Liu, S. Z.; Wu, Y. C.; Cui, Y. X. Single-crystalline lead halide perovskite wafers for high performance photodetectors. *J. Mater. Chem. C* **2019**, *7*, 8357–8363.

[34] Gu, Z. K.; Huang, Z. D.; Li, C.; Li, M. Z.; Song, Y. L. A general printing approach for scalable growth of perovskite single-crystal films. *Sci. Adv.* **2018**, *4*, eaat2390.

[35] Rao, H. S.; Chen, B. X.; Wang, X. D.; Kuang, D. B.; Su, C. Y. A micron-scale laminar $MAPbBr_3$ single crystal for an efficient and stable perovskite solar cell. *Chem. Commun.* **2017**, *53*, 5163–5166.

[36] Edri, E.; Kirmayer, S.; Henning, A.; Mukhopadhyay, S.; Gartsman, K.; Rosenwaks, Y.; Hodes, G.; Cahen, D. Why lead methylammonium tri-iodide perovskite-based solar cells require a mesoporous electron transporting scaffold (but not necessarily a hole conductor). *Nano Lett.* **2014**, *14*, 1000–1004.

[37] He, X. X.; Wang, Y. G.; Li, K.; Wang, X.; Liu, P.; Yang, Y. J.; Liao, Q.; Zhai, T. Y.; Yao, J. N.; Fu, H. B. Oriented growth of ultrathin single crystals of 2D Ruddlesden-Popper hybrid lead iodide perovskites for high-performance photodetectors. *ACS Appl. Mater. Interfaces* **2019**, *11*, 15905–15912.

[38] Huang, Y.; Zhang, Y.; Sun, J. L.; Wang, X. G.; Sun, J. L.; Chen, Q.; Pan, C. F.; Zhou, H. P. The exploration of carrier behavior in the inverted mixed perovskite single-crystal solar cells. *Adv. Mater. Interfaces* **2018**, *5*, 1800224.

[39] He, M.; Li, B.; Cui, X.; Jiang, B. B.; He, Y. J.; Chen, Y. H.; O'Neil, D.; Szymanski, P.; Ei-Sayed, M. A.; Huang, J. S. et al. Meniscus-assisted solution printing of large-grained perovskite films for high-efficiency solar cells. *Nat. Commun.* **2017**, *8*, 16045.

[40] Xiao, Z. G.; Dong, Q. F.; Bi, C.; Shao, Y. C.; Yuan, Y. B.; Huang, J. S. Solvent annealing of perovskite-induced crystal growth for photovoltaic-device efficiency enhancement. *Adv. Mater.* **2014**, *26*, 6503–6509.

[41] Jeon, N. J.; Noh, J. H.; Kim, Y. C.; Yang, W. S.; Ryu, S.; Seok, S. I. Solvent engineering for high-performance inorganic-organic hybrid perovskite solar cells. *Nat. Mater.* **2014**, *13*, 897–903.

[42] Ha, S. T.; Shen, C.; Zhang, J.; Xiong, Q. H. Laser cooling of organic-inorganic lead halide perovskites. *Nat. Photonics* **2016**, *10*, 115–121.

[43] Kamminga, M. E.; Fang, H. H.; Filip, M. R.; Giustino, F.; Baas, J.; Blake, G. R.; Loi, M. A.; Palstra, T. T. M. Confinement effects in low-dimensional lead iodide perovskite hybrids. *Chem. Mater.* **2016**, *28*, 4554–4562.

[44] Gan, L.; He, H. P.; Li, S. X.; Li, J.; Ye, Z. Z. Distinctive excitonic recombination in solution-processed layered organic-inorganic hybrid two-dimensional perovskites. *J. Mater. Chem. C* **2016**, *4*, 10198–10204.

[45] Mitzi, D. B. A layered solution crystal growth technique and the crystal structure of $(C_6H_5C_2H_4NH_3)_2PbCl_4$. *J. Solid State Chem.* **1999**, *145*, 694–704.

[46] Lédée, F.; Trippé-Allard, G.; Diab, H.; Audebert, P.; Garrot, D.; Lauret, J. S.; Deleporte, E. Fast growth of monocrystalline thin films of 2D layered hybrid perovskite. *CrystEngComm* **2017**, *19*, 2598–2602.

[47] Giovanni, D.; Chong, W. K.; Dewi, H. A.; Thirumal, K.; Neogi, I.; Ramesh, R.; Mhaisalkar, S.; Mathews, N.; Sum, T. C. Tunable room-temperature spin-selective optical Stark effect in solution-processed layered halide perovskites. *Sci. Adv.* **2016**, *2*, e1600477.

[48] Calabrese, J.; Jones, N. L.; Harlow, R. L.; Herron, N.; Thorn, D. L.; Wang, Y. Preparation and characterization of layered lead halide compounds. *J. Am. Chem. Soc.* **1991**, *113*, 2328–2330.

[49] Milot, R. L.; Sutton, R. J.; Eperon, G. E.; Haghighirad, A. A.; Martinez Hardigree, J.; Miranda, L.; Snaith, H. J.; Johnston, M. B.; Herz, L. M. Charge-carrier dynamics in 2D hybrid metal-halide perovskites. *Nano Lett.* **2016**, *16*, 7001–7007.

[50] Fu, X. W.; Dong, N.; Lian, G.; Lv, S.; Zhao, T. Y.; Wang, Q. L.; Cui, D. L.; Wong, C. P. High-quality $CH_3NH_3PbI_3$ films obtained via a pressure-assisted space-confined solvent-engineering strategy for ultrasensitive photodetectors. *Nano Lett.* **2018**, *18*, 1213–1220.

[51] Wang, Y. F.; Liu, D. T.; Zhang, P.; Zhang, T.; Ahmad, W.; Ying, X. X.; Wang, F.; Li, J.; Chen, L.; Wu, J. et al. Reveal the growth mechanism in perovskite films via weakly coordinating solvent annealing. *Sci. China Mater.* **2018**, *61*, 1536–1548.

[52] Wang, W. H.; Ma, Y. R.; Qi, L. M. High-performance photodetectors based on organometal halide perovskite nanonets. *Adv. Funct. Mater.* **2017**, *27*, 1603653.

[53] Zhu, P. C.; Gu, S.; Shen, X. P.; Xu, N.; Tan, Y. L.; Zhuang, S. D.; Deng, Y.; Lu, Z. D.; Wang, Z. L.; Zhu, J. Direct conversion of perovskite thin films into nanowires with kinetic control for flexible optoelectronic devices. *Nano Lett.* **2016**, *16*, 871–876.

[54] Deng, W.; Zhang, X. J.; Huang, L. M.; Xu, X. Z.; Wang, L.; Wang, J. C.; Shang, Q. X.; Lee, S. T.; Jie, J. S. Aligned single-crystalline perovskite microwire arrays for high-performance flexible image sensors with long-term stability. *Adv. Mater.* **2016**, *28*, 2201–2208.

[55] Zhuo, S. F.; Zhang, J. F.; Shi, Y. M.; Huang, Y.; Zhang, B. Self-template-directed synthesis of porous perovskite nanowires at room temperature for high-performance visible-light photodetectors. *Angew. Chem., Int. Ed.* **2015**, *54*, 5693–5696.

[56] Zhang, Y.; Du, J.; Wu, X. H.; Zhang, G. Q.; Chu, Y. L.; Liu, D. P.; Zhao, Y. X.; Liang, Z. Q.; Huang, J. Ultrasensitive photodetectors based on island-structured $CH_3NH_3PbI_3$ thin films. *ACS Appl. Mater. Interfaces* **2015**, *7*, 21634–21638.

[57] Chen, K.; Tüysüz, H. Morphology-controlled synthesis of organometal halide perovskite inverse opals. *Angew. Chem., Int. Ed.* **2015**, *54*, 13806–13810.

[58] Zeng, J. P.; Li, X. M.; Wu, Y.; Yang, D. D.; Sun, Z. G.; Song, Z. H.; Wang, H.; Zeng, H. B. Space-confined growth of $CsPbBr_3$ film achieving photodetectors with high performance in all figures of merit. *Adv. Funct. Mater.* **2018**, *28*, 1804394.

[59] Liu, R. H.; Zhou, H.; Song, Z. N.; Yang, X. H.; Wu, D. J.; Song, Z. H.; Wang, H.; Yan, Y. F. Low-reflection, (110)-orientation-preferred $CsPbBr_3$ nanonet films for application in high-performance perovskite photodetectors. *Nanoscale* **2019**, *11*, 9302–9309.

[60] Sutton, R. J.; Eperon, G. E.; Miranda, L.; Parrott, E. S.; Kamino, B. A.; Patel, J. B.; Hörantner, M. T.; Johnston, M. B.; Haghighirad, A. A.; Moore, D. T. et al. Bandgap-tunable cesium lead halide perovskites with high thermal stability for efficient solar cells. *Adv. Energy Mater.* **2016**, *6*, 1502458.

[61] Chang, X. W.; Li, W. P.; Zhu, L. Q.; Liu, H. C.; Geng, H. F.; Xiang, S. S.; Liu, J. M.; Chen, H. N. Carbon-based $CsPbBr_3$ perovskite solar cells: All-ambient processes and high thermal stability. *ACS Appl. Mater. Interfaces* **2016**, *8*, 33649–33655.

[62] Zuo, Z. Y.; Ding, J. X.; Zhao, Y.; Du, S. J.; Li, Y. F.; Zhan, X. Y.; Cui, H. Z. Enhanced optoelectronic performance on the (110) lattice plane of an $MAPbBr_3$ single crystal. *J. Phys. Chem. Lett.* **2017**, *8*, 684–689.

[63] Mao, J.; Sha, W. E. I.; Zhang, H.; Ren, X. G.; Zhuang, J. Q.; Roy, V. A. L.; Wong, K. S.; Choy, W. C. H. Novel direct nanopatterning approach to fabricate periodically nanostructured perovskite for optoelectronic applications. *Adv. Funct. Mater.* **2017**, *27*, 1606525.

[64] Lee, L.; Baek, J. M.; Park, K. S.; Lee, Y. E.; Shrestha, N. K.; Sung, M. M. Wafer-scale single-crystal perovskite patterned thin films based on geometrically-confined lateral crystal growth. *Nat. Commun.* **2017**, *8*, 15882.

[65] Yang, J. L.; Siempelkamp, B. D.; Liu, D. Y.; Kelly, T. L. Investigation of $CH_3NH_3PbI_3$ degradation rates and mechanisms in controlled humidity environments using *in situ* techniques. *ACS Nano* **2015**, *9*, 1955–1963.

[66] Yang, S.; Wang, Y.; Liu, P. R.; Cheng, Y. B.; Zhao, H. J.; Yang, H. G. Functionalization of perovskite thin films with moisture-tolerant molecules. *Nat. Energy* **2016**, *1*, 15016.

[67] Christians, J. A.; Miranda Herrera, P. A.; Kamat, P. V. Transformation of the excited state and photovoltaic efficiency of $CH_3NH_3PbI_3$ perovskite upon controlled exposure to humidified air. *J. Am. Chem. Soc.* **2015**, *137*, 1530–1538.

[68] Mateker, W. R.; McGehee, M. D. Progress in understanding degradation mechanisms and improving stability in organic photovoltaics. *Adv. Mater.* **2017**, *29*, 1603940.

[69] Han, Y.; Meyer, S.; Dkhissi, Y.; Weber, K.; Pringle, J. M.; Bach, U.; Spiccia, L.; Cheng, Y. B. Degradation observations of encapsulated planar $CH_3NH_3PbI_3$ perovskite solar cells at high temperatures and humidity. *J. Mater. Chem. A* **2015**, *3*, 8139–8147.

[70] Li, X.; Tschumi, M.; Han, H. W.; Babkair, S. S.; Alzubaydi, R. A.; Ansari, A. A.; Habib, S. S.; Nazeeruddin, M. K.; Zakeeruddin, S. M.; Grätzel, M. Outdoor performance and stability under elevated temperatures and long-term light soaking of triple-layer mesoporous perovskite photovoltaics. *Energy Technol.* **2015**, *3*, 551–555.

[71] Aristidou, N.; Eames, C.; Sanchez-Molina, I.; Bu, X. N.; Kosco, J.; Islam, M. S.; Haque, S. A. Fast oxygen diffusion and iodide defects mediate oxygen-induced degradation of perovskite solar cells. *Nat. Commun.* **2017**, *8*, 15218.

[72] Zhao, J. J.; Deng, Y. H.; Wei, H. T.; Zheng, X. P.; Yu, Z. H.; Shao, Y. C.; Shield, J. E.; Huang, J. S. Strained hybrid perovskite thin films and their impact on the intrinsic stability of perovskite solar cells. *Sci. Adv.* **2017**, *3*, eaao5616.

[73] Wu, Y. Z.; Yang, X. D.; Chen, W.; Yue, Y. F.; Cai, M. L.; Xie, F. X.; Bi, E. B.; Islam, A.; Han, L. Y. Perovskite solar cells with 18.21% efficiency and area over 1 $cm^2$ fabricated by heterojunction engineering. *Nat. Energy* **2016**, *1*, 16148.

[74] Li, B.; Zhang, Y. N.; Zhang, L. Y.; Yin, L. W. Graded heterojunction engineering for hole-conductor-free perovskite solar cells with high hole extraction efficiency and conductivity. *Adv. Mater.* **2017**, *29*, 1701221.

[75] Li, W. G.; Wang, X. D.; Liao, J. F.; Wei, Z. F.; Xu, Y. F.; Chen, H. Y.; Kuang, D. B. A laminar $MAPbBr_3$/$MAPbBr_{3-x}I_x$ graded heterojunction single crystal for enhancing charge extraction and optoelectronic performance. *J. Mater. Chem. C* **2019**, *7*, 5670–5676.

[76] Wei, W.; Zhang, Y.; Xu, Q.; Wei, H. T.; Fang, Y. J.; Wang, Q.; Deng, Y. H.; Li, T.; Gruverman, A.; Cao, L. et al. Monolithic integration of hybrid perovskite single crystals with heterogenous substrate for highly sensitive X-ray imaging. *Nat. Photonics* **2017**, *11*, 315–321.

[77] Shaikh, P. A.; Shi, D.; Retamal, J. R. D.; Sheikh, A. D.; Haque, M. A.; Kang, C. F.; He, J. H.; Bakr, O. M.; Wu, T. Schottky junctions on perovskite single crystals: Light-modulated dielectric constant and self-biased photodetection. *J. Mater. Chem. C* **2016**, *4*, 8304–8312.

[78] Bai, Y.; Zhang, H. X.; Zhang, M. J.; Wang, D.; Zeng, H.; Zhao, J.; Xue, H.; Wu, G. Z.; Su, J.; Xie, Y. et al. Liquid-phase growth and optoelectronic properties of two-dimensional hybrid perovskites $CH_3NH_3PbX_3$ (X = Cl, Br, I). *Nanoscale* **2020**, *12*, 1100–1108.

[79] Gui, P. B.; Zhou, H.; Yao, F.; Song, Z. H.; Li, B. R.; Fang, G. J. Space-confined growth of individual wide bandgap single crystal $CsPbCl_3$ microplatelet for near-ultraviolet photodetection. *Small* **2019**, *15*, 1902618.